





RESEARCH ARTICLE OPEN ACCESS

Coeval Transverse and Axial Sediment Delivery to the Northern Hikurangi Trough During the Late Quaternary

Anthony E. Shorrock¹  | Lorna J. Strachan¹ | Philip M. Barnes²  | Gregory F. Moore³ | Adam D. McArthur⁴  | Davide Gamboa⁵  | Adam D. Woodhouse⁶ | Rebecca E. Bell⁷ | Sam R. Davidson² | Helen C. Bostock⁸

¹School of Environment, University of Auckland, Auckland, New Zealand | ²National Institute of Water and Atmospheric Research (NIWA), Wellington, New Zealand | ³Department of Earth Sciences, University of Hawaii, Honolulu, Hawaii, USA | ⁴School of Earth and Environment, University of Leeds, Leeds, UK | ⁵CESAM and Department of Geosciences, Universidade de Aveiro, Aveiro, Portugal | ⁶School of Earth and Environmental Sciences, Cardiff University, Cardiff, UK | ⁷Department of Earth Science & Engineering, Imperial College London, London, UK | ⁸School of Environment, University of Queensland, Brisbane, Queensland, Australia

Correspondence: Anthony E. Shorrock (anthony.shorrock@auckland.ac.nz)

Received: 3 September 2024 | **Revised:** 24 January 2025 | **Accepted:** 25 January 2025

Funding: Funding for this project is from a University of Auckland Doctoral Scholarship and the Marsden Fund of the Royal Society Te Apārangi (PI Lorna Strachan, 20-UOA-099). D. Gamboa thanks the financial support to CESAM by the Portuguese Fundação para a Ciência e a Tecnologia (FCT) I.P./MCTES through national funds (PIDDAC) UIDP/50017/2020, UIDB/50017/2020 and LA/P/0094/2020.

Keywords: axial channels | glacio-eustatic cycles | gravity flows | hikurangi | IODP | quaternary sedimentation | subduction trench | transverse canyons

ABSTRACT

Subduction trenches receive sediment from sediment gravity flows sourced from transverse pathways and trench parallel axial transport pathways. Understanding the interplay between axial and transverse sediment transport in shaping stratigraphic architectures is hindered by the episodic nature of sedimentary gravity flows and limited datasets, yet such insights are crucial for reconstructing sedimentary flow pathways and interpreting sedimentary records. We investigate sediment routing pathways to the northern Hikurangi Trough of New Zealand using a combination of multibeam, 2D and 3D seismic reflection and International Ocean Discovery Program core data from Site U1520. Site U1520's location downstream of axial and transverse conduits of sediment delivery makes it an excellent location to observe how these processes interact in deep marine settings. We characterise regional basin floor geomorphology and sub-surface architecture of the upper ~110 m siliciclastic sequence of the Hikurangi Trough deposited over the past ~42 ka (Seismic Unit 1; SU1). Sediment delivery to the trough is fed by sediment gravity flows sourced from both the shelf-incising transverse Māhia Canyon to the south-west and the axial Hikurangi Channel to the south. Flows sourced from these systems have a strong influence on the geomorphology of the region and are responsible for forming large-scale bathymetric features such as erosional scours and sediment waves. Sedimentary features identified within SU1 indicate that sediment transport via the transverse Māhia Canyon was more significant than that of the axial Hikurangi Channel throughout the last 42 ka, particularly during the last glacial period when sea levels were lower, and sedimentation rates were extremely high (up to ~20 m/kyr). This study emphasises the need for a nuanced consideration of transverse and axial systems and how they may influence sediment records and the geomorphic characteristics of trench systems.

1 | Introduction

Subduction trench systems are commonly fed by a mix of transverse sediment transport perpendicular to the main axis of the

depo-center and axial sediment transport parallel to the main axis (Underwood 1986, 2007, 2023; Bailleul et al. 2007, 2013; Buchs et al. 2015; McArthur and Tek 2021; Figure 1). Subduction trenches can be either erosional or aggradational, the latter forming troughs

This is an open access article under the terms of the [Creative Commons Attribution](https://creativecommons.org/licenses/by/4.0/) License, which permits use, distribution and reproduction in any medium, provided the original work is properly cited.

© 2025 The Author(s). *Basin Research* published by International Association of Sedimentologists and European Association of Geoscientists and Engineers and John Wiley & Sons Ltd.

Summary

- Transverse sediment delivery has been the primary driver of sediment accumulation in the northern Hikurangi Trough over the past 42,000 years, particularly during the sea level lowstand of MIS2.
- The formation of large-scale bedforms, including sediment waves and erosional scours, are linked to sedimentary gravity flows from the Māhia Canyon.
- Axial sediment transport via the Hikurangi Channel has contributed but is less significant in comparison to transverse flows.
- The study highlights the need to consider the interplay of transverse and axial sedimentation in interpreting sedimentological and paleoclimate records in the Hikurangi Trough, and in other subduction trenches around the world.

composed of thick (up to ~8 km) siliciclastic sediment successions (Lewis, Collot, and Lalle 1998; Heuret et al. 2012; Brizzi et al. 2020; McArthur and Tek 2021). The precise mechanisms of sediment delivery, their relative importance and their interactions, ultimately control the composition and stratigraphic architecture of basin floor sequences (Stow 1985; Bourget et al. 2010, 2011; Sømme, Martinsen, and Thurmond 2009; Covault and Graham 2010; Tek et al. 2021; McArthur et al. 2022). Variations in the composition and stratigraphic architecture of trench sequences may, in turn, influence the composition, structure, mechanics and hydrogeology of accretionary wedges (Skarbak, Rempel, and Schmidt 2012; Saffer and Wallace 2015; Barnes et al. 2020). However, disentangling the role of axial versus transverse sediment transport and the differences in the resulting stratigraphic architectures of these systems remains challenging due to the episodic nature of sedimentary gravity flows hampering the ability for researchers to directly observe such events, alongside the paucity of datasets that allow for reconstruction of sedimentary flow pathways (Talling et al. 2015).

Transverse systems in subduction trench settings generally refer to channel systems perpendicular to the margin and deliver sediment down the slope and into the trench system (Figure 1). On the Hikurangi Subduction Margin (HSM) many of these transverse systems are expressed in the form of canyons that incise the edge of the continental shelf and slope flowing into the Hikurangi Trough (Lewis, Collot, and Lalle 1998; Pedley et al. 2010; Chow, Kaneko, and Townend 2022; Figures 1 and 2). Axial channel systems transport sediments along the trench and often evolve temporally and spatially as channels propagate and migrate along the internal longitudinal axis of a trench due to different tectonic or climatic drivers (McArthur and Tek 2021). They are thought to occur when sediment supply to a trench is high enough to suppress the expression of the underlying rugosity, permitting uninterrupted axial flow and channelisation (Underwood and Karig 1980; McArthur and Tek 2021). Axial channels are typically sourced from transverse systems along the continental margin that combine into the larger regional system; however, the relative influence of axial versus transverse sediment transport can vary significantly,

especially with proximity to the mouths of major submarine canyon systems.

Trench-hosted sediment successions are commonly dominated by gravity flow deposits as a result of active tectonics resulting in rapid uplift and erosion of rocks and reworking of sediments which may be sourced and dispersed through transverse and axial drainages (Piper, von Huene, and Duncan 1973; Underwood and Karig 1980; Lewis, Collot, and Lalle 1998; Bourget et al. 2011; Covault et al. 2012; McArthur and Tek 2021; Underwood 2023). Glacio-eustatic sea level cycles can have a profound effect on the sediment supply, the dominant mode of sediment delivery and the sedimentation rates in subduction zones (Zuffa et al. 2000; Paull et al. 2014; McArthur and Tek 2021; Woodhouse et al. 2022). In New Zealand, environmental conditions during peak glacial periods resulted in enhanced connectivity between terrestrial river systems and submarine canyons due to lower sea levels, as well as increased levels of erosion due to cooler, drier conditions with reduced vegetation cover (Alloway et al. 2007; Upton et al. 2013; Woodhouse et al. 2022).

International Ocean Drilling Program (IODP) Expedition 375 Site U1520 in the northern HSM (Figures 2 and 3) lies in proximity to both transverse and axial sediment transport systems, making this an excellent location to understand the interaction of both drainages. This includes the ~70 km long, shelf-incising Māhia Canyon, a tri-branching, shelf-incising transverse canyon system that acts as a conduit of sediments sourced from the continental shelf and slope directly to the trough floor, with the mouth of the canyon being orientated towards Site U1520 (Pedley et al. 2010; Chow, Kaneko, and Townend 2022; Figure 3A). The Māhia Canyon is connected to the Paritu Trough on the continental slope, which also feeds the Paritu Channel (Pouderoux et al. 2012; Figure 3). The Paritu Channel is constrained to the south by the relief of the neighbouring Paritu Debris Avalanche, with sediment gravity flows funnelled into the Lower Paritu Basin, rather than flowing into the Māhia Canyon (Pouderoux et al. 2012; Figure 3). The Hikurangi Channel is a ~1500 km-long axial channel fed by numerous shelf-incising transverse canyon systems located along the continental slope of the HSM; Site U1520 is located directly northwards of a conspicuous easterly bend in the channel and the northward overspill of flows rounding this bend would likely reach Site U1520 (Lewis, Collot, and Lalle 1998; Collot et al. 2001; McArthur and Tek 2021; Figures 2 and 3).

In this study, we use multibeam bathymetric data integrated with 2D and 3D seismic reflection data from the northern HSM, tied to IODP Site U1520 drilling data, to determine the interplay between axial and transverse drainages. Through the analysis of both the modern geomorphic expression of the seafloor, coupled with subsurface seismic facies analyses, we reconstruct the sediment transport pathways towards Site U1520 and how they have changed over time. Integration with high-resolution age control has allowed us to document the evolution of this northern HSM sequence over the past ~42 ka, covering Marine Isotope Stages (MIS) 3, 2 and 1. Such insights are important for understanding the stratigraphic architecture of subduction trench sequences, but additionally is critical to understanding the important paleorecords of past earthquakes (e.g., Howarth et al. 2021), sea level, climate changes (e.g., Woodhouse et al. 2022) and the ability to

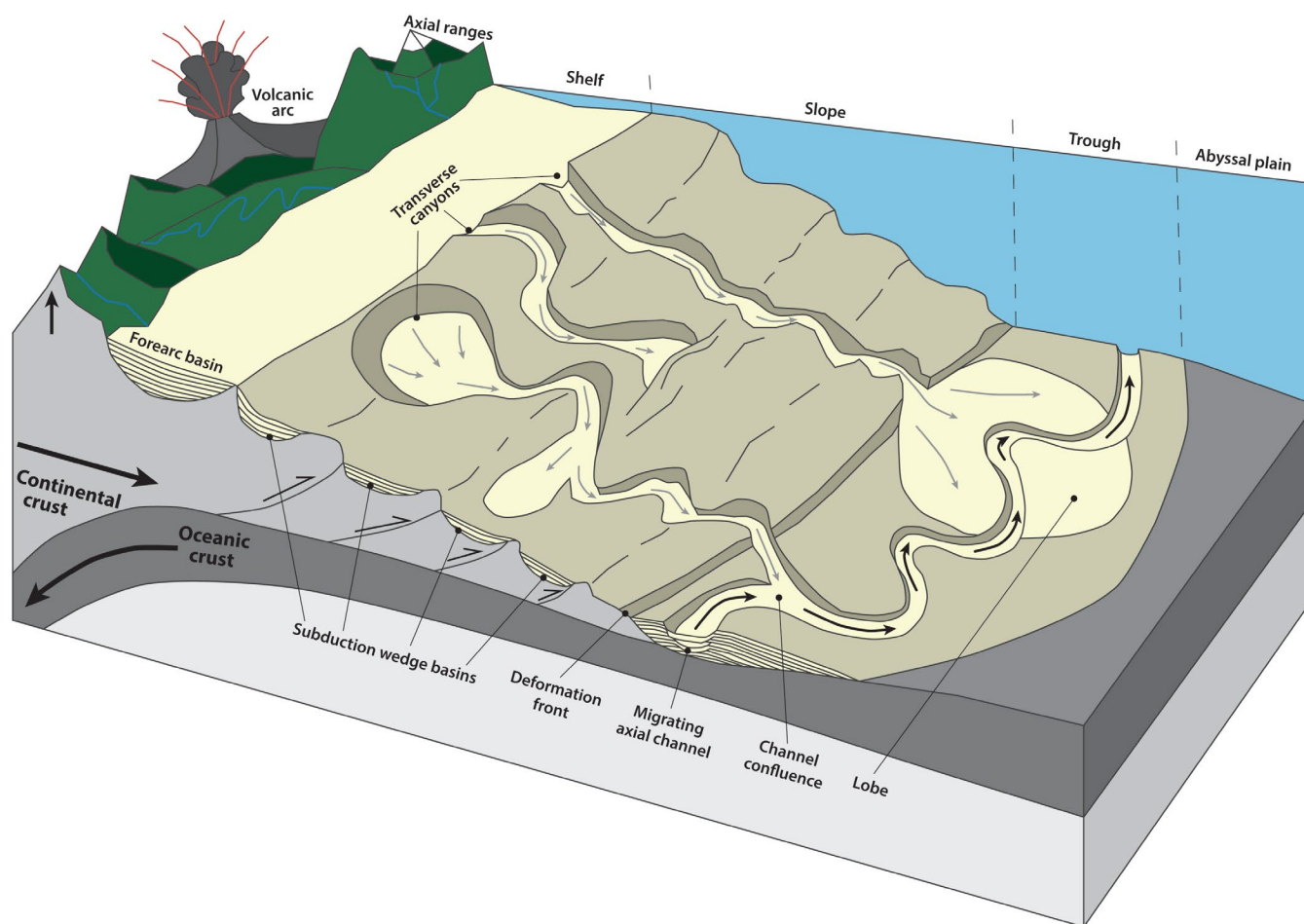


FIGURE 1 | Idealised schematic (not to scale) displaying axial and transverse sediment transport systems along an aggradational subduction margin. Individual transverse systems (typically in the form of slope-incising canyons) transport sediment from the continental shelf and slope into wider axial channel systems on the trough floor.

capture organic carbon (e.g., Omura et al. 2017) and pollutants (e.g., Kane et al. 2020).

2 | Geological Setting

The Hikurangi Trough is a northeast-southwest-orientated trench associated with the HSM off the east coast of Aotearoa New Zealand, formed by oblique subduction of the oceanic Pacific Plate beneath the continental Australian Plate (Lewis 1993; Barnes et al. 2010; Mochizuki et al. 2019). The northern margin is steep and scarred with indentations due to past seamount subduction; these indentations host several submarine canyons and channel systems (e.g., Pedley et al. 2010; Ellis et al. 2015; Barnes et al. 2018; Davidson et al. 2020).

The northern Hikurangi Trough is filled by a ~1 km thick siliciclastic sequence thought to have been deposited during the past <3.5 Ma (Lewis, Collot, and Lalle 1998; Barnes et al. 2010; Plaza-Faverola et al. 2012; Ghisetti et al. 2016; Kroeger et al. 2019). Sediment gravity flows are the dominant mechanism of sediment delivery to the Hikurangi Trough (Lewis 1994; Lewis, Collot, and Lalle 1998; Orpin 2004; Pedley et al. 2010; Mountjoy et al. 2018; Couvin et al. 2020; Watson, Mountjoy, and Crutchley 2020; McArthur and Tek 2021; Tek et al. 2021).

This study focuses on the basin floor of the northern Hikurangi Trough, ~95 km east of the coast of the Raukūmara Peninsula (Figures 2 and 3). The study area is characterised by an extensive, gently northward-dipping sedimentary plain constrained between the edge of the continental slope to the west and by seamounts to the east (Barnes et al. 2019; Figure 3). The northern limit is constrained by the Ruatōria Debris Avalanche, formed by the collapse of the continental slope (Lewis, Collot, and Lalle 1998). An extensive siliciclastic mass transport deposit (MTD) associated with the Ruatōria Debris Avalanche directly underlies the study area, henceforth referred to as the Ruatōria Mass Transport Deposit (RMTD) (Lewis, Collot, and Lalle 1998; Collot et al. 2001; Barnes et al. 2019; Underwood 2023).

Here, we focus on the previously described Seismic Unit 1 (SU1, Barnes et al. 2019; Figure 3B), which aligns with lithologic Unit I of Well D at Site U1520 (Barnes et al. 2019; Woodhouse et al. 2022; Noda et al. 2024; Underwood 2023). Site U1520 is located ~16 km east of the continental slope and ~4 km west of the Tūrangānuī Knoll at a water depth of 3520 mbsl (Saffer et al. 2019; Barnes et al. 2019). The site is located about 30 km north of the Hikurangi Channel and the mouth of the Māhia Canyon, and 65 km south of the Ruatōria Debris Avalanche (Lewis, Collot, and Lalle 1998; Collot et al. 2001; Pedley

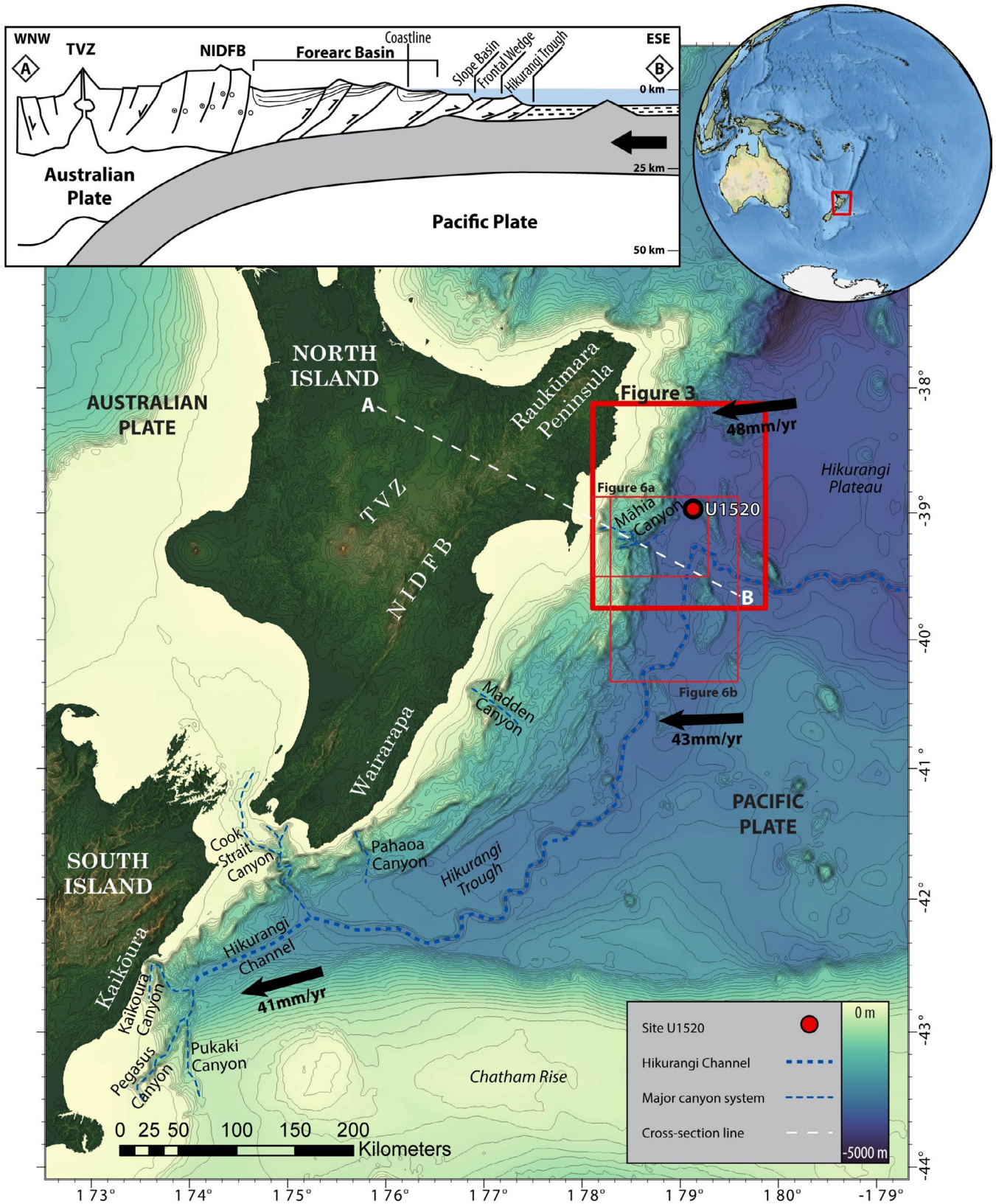


FIGURE 2 | Location map displaying the key tectonic and geomorphic features along the Hikurangi Subduction Margin, and the extent of Figures 3 and 6A,B. Plate motion vectors are indicated by black arrows (Wallace et al. 2004). The upper left inset shows a schematic cross-section (not to scale) of the tectonic setting across lines A–B, showing the relationship between the subducting Pacific Plate and the over-riding Australian Plate (adapted from Pedley et al. 2010). NIDFB=North Island Dextral Fault Belt; TVZ=Taupo Volcanic Zone.

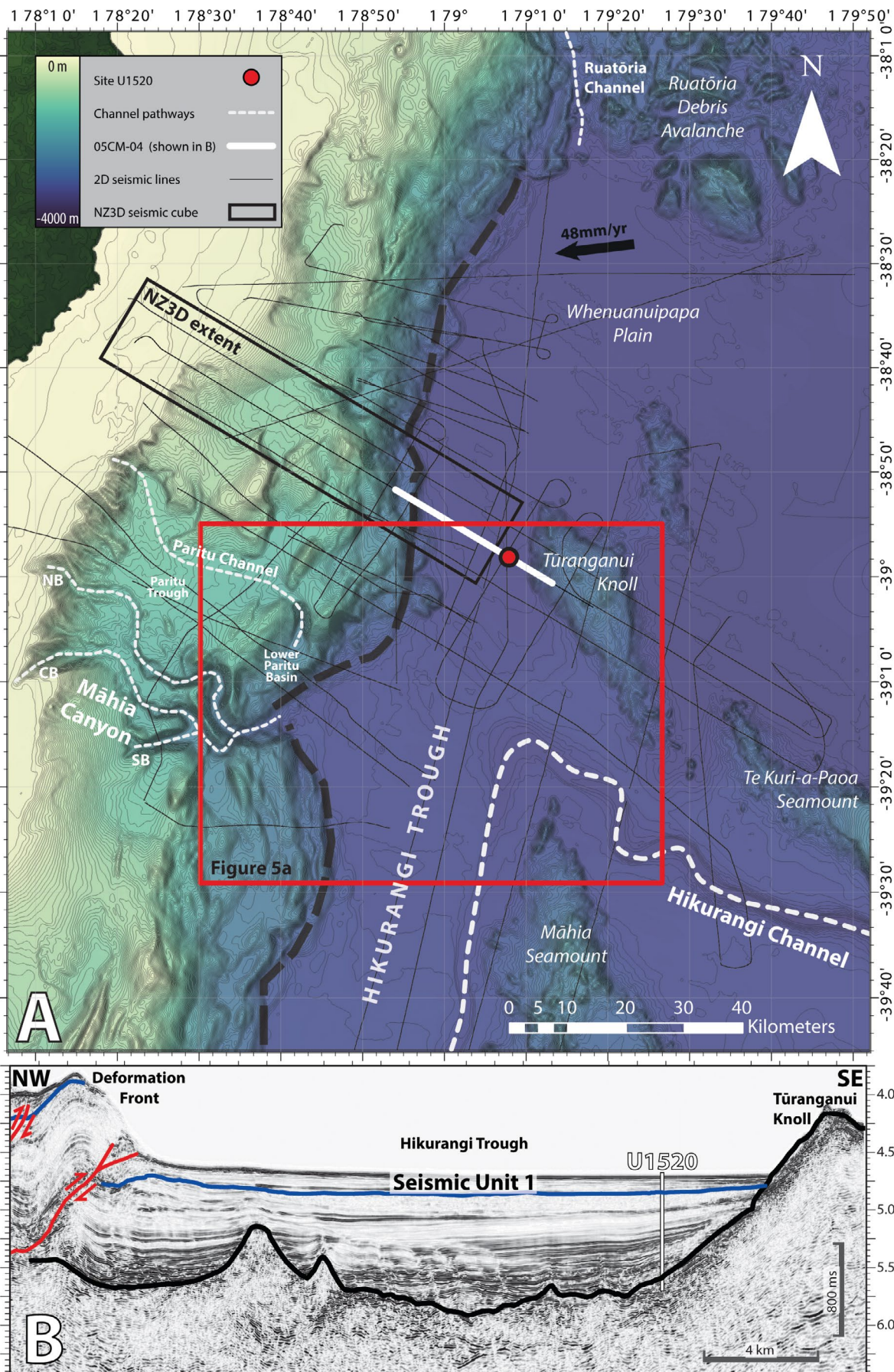


FIGURE 3 | Legend on next page.

FIGURE 3 | (A) Regional bathymetric map of the northeastern HSM showing the extent of the Māhia Canyon alongside minor channel systems in the study region and the spatial extent of both 2D and 3D seismic surveys utilised by this study. The black dashed line represents the subduction front. See [Supporting Information](#) for labelled maps of 2D seismic surveys used in this study. (B) Regional seismic section 05CM-04 (Bell et al. 2010; Barker et al. 2018; Barnes et al. 2020) crossing northern Hikurangi Trough across IODP Site U1520, showing Seismic Unit 1. The blue line is the base of SU1, the red lines are thrust faults on the subduction front and the black line shows the morphology of the volcanic basement layer.

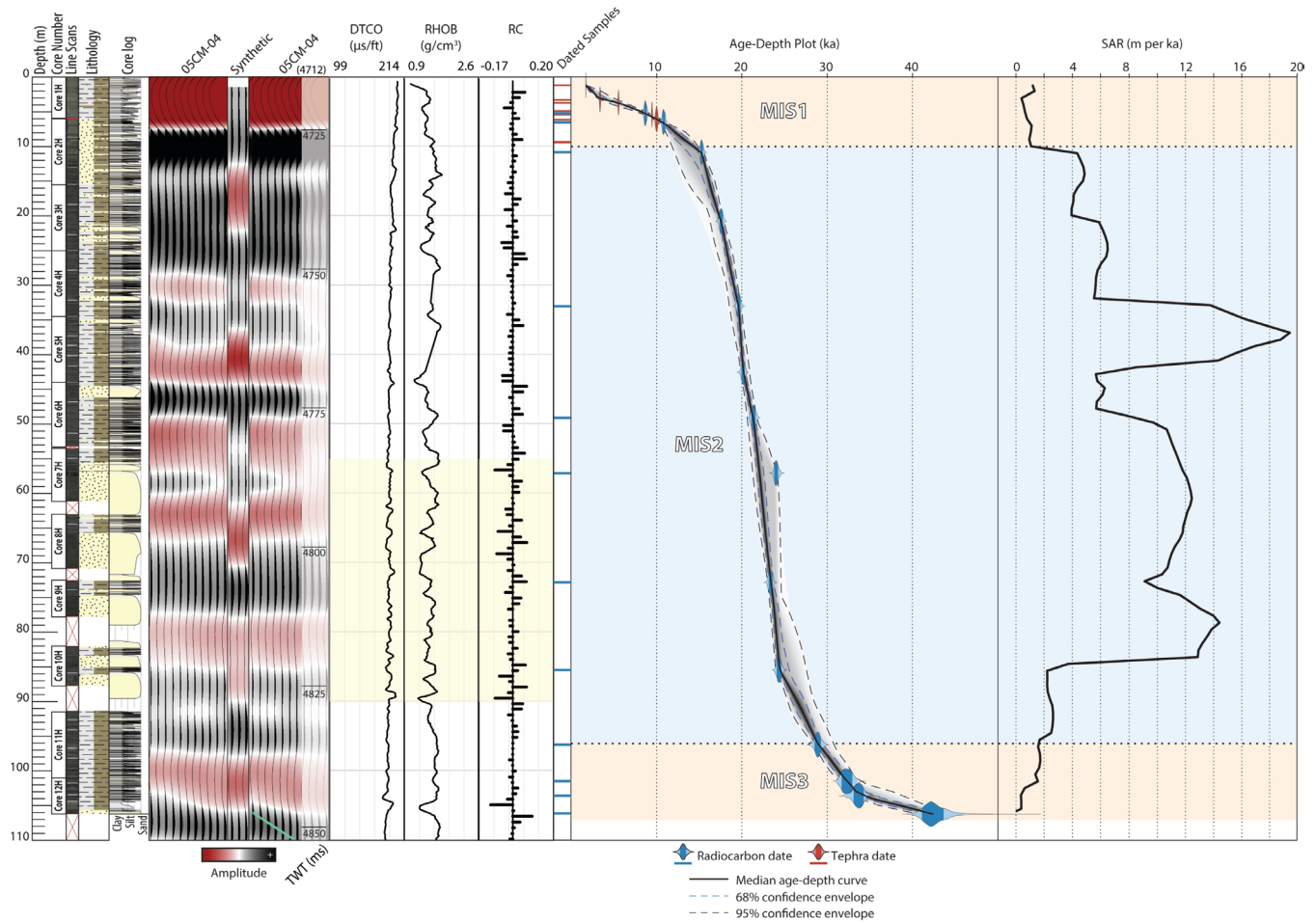


FIGURE 4 | Downcore log from Site U1520 with the seismic well-tie, Lithological and Compressional Slowness (DTCO) log, density log (RHOB), reflection coefficients (RC), age-depth plot and sediment accumulation rate (SAR) (updated from Woodhouse et al. 2022). The yellow background highlight between 55 and 90 mbsf indicates the presence of thick sand beds. Inputs for the age-depth model are provided in Table S2.

et al. 2010; Barnes et al. 2019, Figure 3). Unit I is ~110 m thick and is composed of stacked silt-and-sand dominated beds that were deposited during the last ~42 ka alongside minor clays and tephra (Barnes et al. 2019; Woodhouse et al. 2022). The beds have been interpreted as a sequence comprised of turbidites, debrites, mixed turbidite-contourites and hemipelagites (Barnes et al. 2019; Noda et al. 2024; Woodhouse et al. 2022; Underwood 2023).

3 | Data Sets and Methodology

High-resolution (25 m grid) bathymetric data were collected by the RV *Tangaroa* across the study region using Kongsberg SIMRAD EM 300/302 multi-beam echo sounders (Lewis 2001; Barnes et al. 2011; Figure 3A). ESRI's ArcGIS suite was used to view and undertake spatial analysis of the datasets to characterise

the seafloor geomorphology of the Hikurangi Trough and the surrounding area. A method outlined in Shumaker et al. (2018) was applied to extract morphometric scaling relationships from a northward stretch of the Hikurangi Channel and three branches of the Māhia Canyon using MATLAB. Channel thalwegs were generated using the stream network analysis toolkit in ArcGIS and channel margins were visually mapped. These morphometric measurements of channels can be used to constrain the interpretation of the flow processes that create them (Shumaker et al. 2018).

We used post-stack time-migrated 2D seismic reflection data acquired from seven surveys conducted between 1972 and 2015 (Figure 3A). For details on seismic data acquisition and processing refer to Barker et al. (2009), Pedley et al. (2010), Wallace et al. (2019); Barnes et al. (2020) and Wang et al. (2022). Additionally, we used new high-resolution

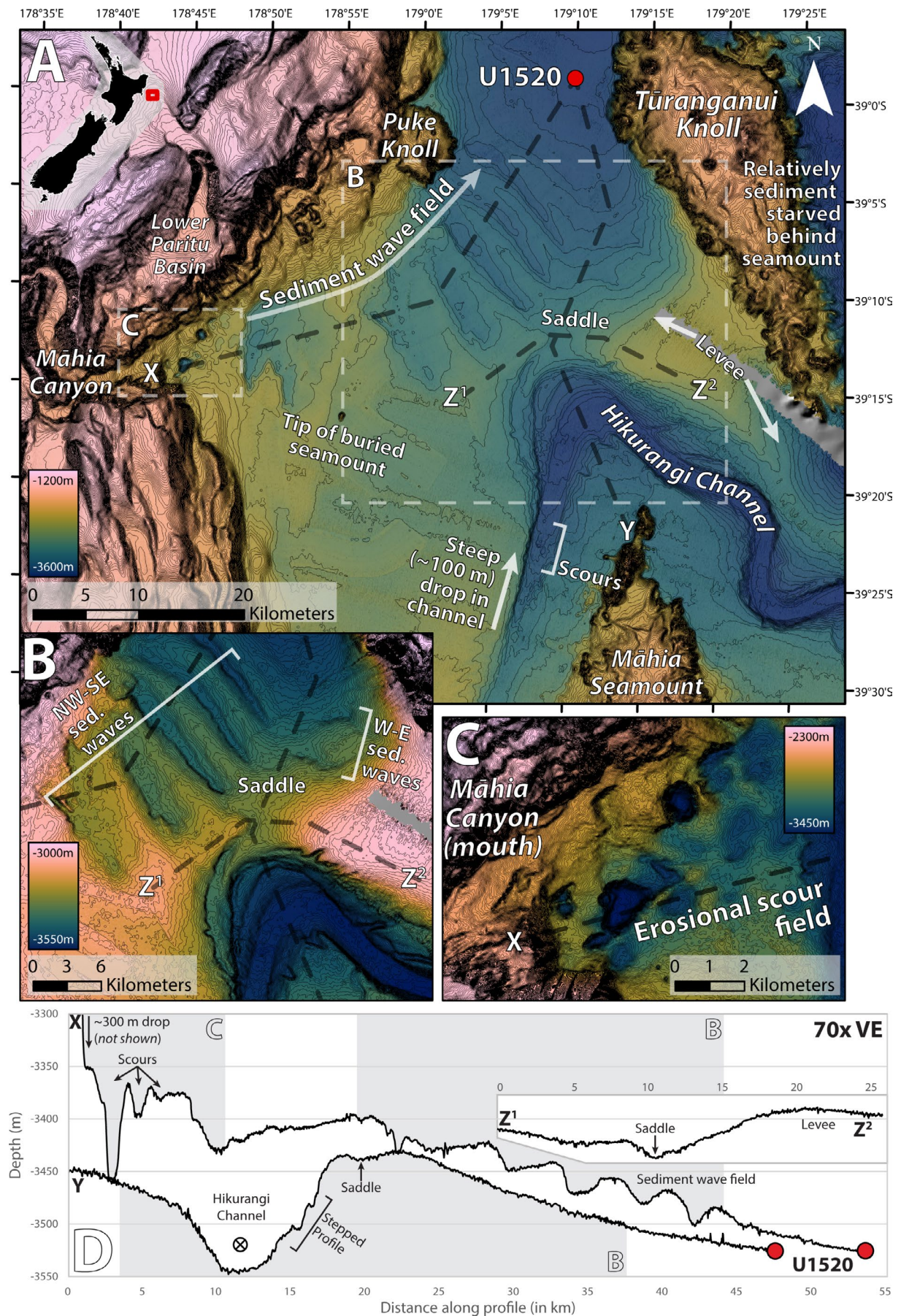


FIGURE 5 | (A) Map of the morphology of the study area. (B) Inset showing the Hikurangi Channel bend, saddle and the Māhia wave field. (C) Inset of the erosional scour field at the mouth of the Māhia Canyon. (D) Elevation profiles across key features in the study region.

parametric sediment echo-sounder data that were acquired with a hull-mounted Topographic Parametric Sonar (TOPAS) 18 sub-bottom profiler during TAN2207 (Maier et al. 2022). This data provide higher-resolution sub-surface imaging of the seafloor than can be resolved from traditional 2D seismic reflection data, albeit to a significantly shallower depth. The 2D seismic reflection and TOPAS data were interpreted in SLB's software Petrel 2016.

In addition, we also examined vertical profiles and depth slices from the 15×60 km NZ3D seismic volume (Bangs et al. 2022a, 2022b, 2023; Gase et al. 2023; Figure 3A). These data were commercially processed with 3D full wave-form inversion and pre-stack depth migration, with inline spacing of 18.75 m and crossline spacing of 12.5 m (see Bangs et al. 2023 for further details).

Logging-while-drilling (LWD) data are available for site U1520 in the interval of interest and were used to produce a synthetic seismic trace for core-log-seismic integration (Barnes et al. 2019). Check-shot data are not available for any of the drill sites. Sonic logs measured in microsec/ft. were converted to compressional velocity (V_p) logs in m/s. Sourceless neutron-gamma density logs provided density information in g/cm^3 . These V_p and density logs were multiplied to produce acoustic impedance logs, from which reflection coefficient logs can be derived (Barnes et al. 2019). A Ricker source wavelet with a frequency of 25 Hz (to mimic the dominant frequency of the 05CM seismic data) was convolved with the reflection coefficient log to produce a synthetic seismic trace to tie the logging data from Site U1520 with seismic line 05CM-04 (Figures 3 and 4). In lieu of check-shot data, this seismic-well-tie enabled the correlation of seismic data, which is recorded in two-way time (TWT), with core and LWD data, which is recorded in depth, and the development of an accurate time–depth relationship (Pecher et al. 2018; Barnes et al. 2019; Wallace et al. 2019; Figure 4). The time–depth relationship provided by the seismic-well-tie was used to create a velocity model for the interval of interest, which was then used to convert the domain of seismic lines from TWT to depth (m) to construct a regional isopach thickness map. Comparing the calculated thickness of SU1 (108.9 m) with that of Lithologic Unit I (110 m) at Site U1520 suggests an error percentage of 0.99% (Barnes et al. 2019). The seismic-well-tie also allows for chronostratigraphic models of core U1520D (Crundwell and Woodhouse 2022; Woodhouse et al. 2022; Figure 4) to be directly correlated with seismic stratigraphic features.

Subunits and seismic facies were identified based on seismic reflection characteristics (architecture, reflection configuration, continuity and amplitude). These facies are used to interpret depositional processes and paleoenvironments linked to the core sediments (Sangree and Widmier 1979; Mitchum Jr 1977; Reading 1996; Veeken and Van Moerkerken 2013).

4 | Results

4.1 | Modern Seafloor Geomorphology

The Māhia Canyon, the Hikurangi Channel and sets of large-scale waveforms are the most significant features that

characterise the modern geomorphology of the northern Hikurangi Trough; here we provide detailed observations of these features and interpretations of their formation.

4.1.1 | Māhia Canyon

4.1.1.1 | Observations. The geometry of Māhia Canyon is characterised by shallow gullies towards the continental shelf and upper slope that transition into a tri-branching (northern, central and southern) sinuous canyon with ~450 m high walls constraining a canyon floor that varies from U-shaped to V-shaped (Figures 5 and 6). Aspect ratios (the ratio of channel width to depth) of all mapped branches of the Māhia Canyon are low, with median values ranging from 5.07 to 7.52. The northern branch includes the lower section following the confluence of the other branches and represents a full transect of the canyon from the edge of the shelf to the trough floor, is described below. The central and southern branches, which represent shorter transects prior to the confluence of all three branches, are described in the [Supporting Information](#).

The northern branch runs eastwards for ~50 km down the continental slope before reaching the Hikurangi Trough floor, after which it almost completely loses confinement (water depths –1500 to –3450 m) (Figure 6A). In the longitudinal profile, the slope trends smoothly except for some minor (> 50 m) steps (Figure 6B²). It is steep with an average slope of 3.09° and canyon depth progressively increases from ~100 to > 700 m (Figure 6A^{1,2}). The canyon shape morphs from a U-shaped (~4 km wide and ~100 m deep) upslope to a V-shaped (~2 km wide and ~450 m deep) at ~20 km downstream (Figure 6A¹). The canyon then begins to widen towards the base where the mouth of the canyon opens into the Hikurangi Trough to > 6 km width and > 700 m deep, back into a U-shape (Figure 6A¹). This branch is sinuous (1.55) due to sharp bends in the mid-slope (Figure 6A).

There is a steep (8.5°) ~300 m drop in the slope of the Māhia Canyon as it opens into the Hikurangi Trough; at the base of this drop, the trough floor hosts a field of enclosed topographic depressions that have circular-to-oval shapes of up to ~1.5 km wide and ~90 m deep (Figure 5).

4.1.1.2 | Interpretations. The low aspect ratios in all branches of the canyon suggest that their ability to confine turbidity currents is high (Shumaker et al. 2018). The steep gradients of the canyon branches would facilitate high flow velocities, with observations from other submarine canyon settings (e.g., Gaoping Canyon) measuring flow speeds as high as 16 m/s (Talling et al. 2023). Such flows are potentially highly erosive and super-critical in nature, which would contribute to the deeply incised morphology observed on the lower slope (Sequeiros 2012). This is supported by prior studies of the Māhia Canyon that have noted the presence of erosional headscarps along the canyon margins, alongside slumps from the canyon walls (Pedley et al. 2010). The minor steps observed on the downstream longitudinal profiles are interpreted as knick-points associated with thrust faults propagating across the canyon floors (Pedley et al. 2010). Towards the mouth of the canyon, the cross-sectional profiles of the canyon display large-scale incisions and stepped profiles,

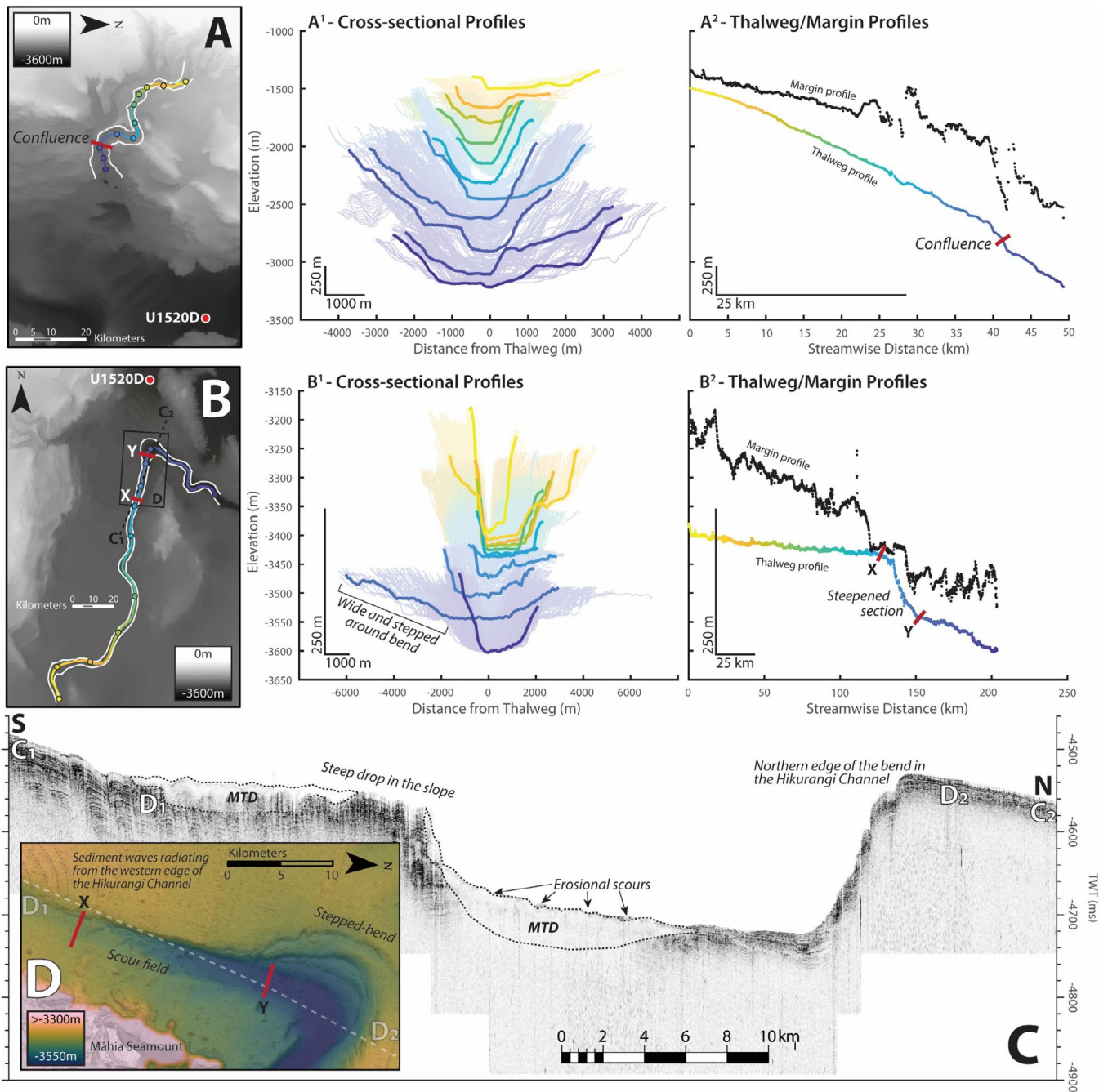


FIGURE 6 | (A) Location, cross-sectional profiles (A¹) and thalweg/margin profiles (A²) of the northern branch of the Māhia Canyon. See Figure S2 for central and southern branches. (B) Location, cross-sectional profiles (B¹) and thalweg/margin profiles (B²) of a ~100 km section of the Hikurangi Channel leading up and around the bend. Labels X and Y show the beginning and end of a steepened section of the channel, also shown in (C). (C) TAN2207 TOPAS echo sounder line across the steep drop in the channel profile, highlighting the occurrence of MTDs within the channel. The location of the line is shown in (B) (C₁–C₂), as the locations of points D₁–D₂. (D) Inset showing overbank sediment waves, erosional scours and the bend of the Hikurangi Channel. See Figure S4 for elevation profiles of these features.

possibly indicating preferential erosion within the flow paths of downslope currents (Figure 5C,D).

The topographic depressions at the mouth of the canyon where it exits into the trough are consistent with large-scale erosional scours (sensu Symons et al. 2016; Figure 5C). Symons et al. (2016) describe two possible causes: (a) they are formed by excavation of defects in the initial bedding plane(s) or (b)

they are associated with supercritical flows in which scours are formed by hydraulic jumps caused by flow expansion or breaks in slope. Alternatively, Pohl et al. (2019) suggest that (c) ‘flow relaxation’ can form scours due to the change in pressure gradient at the toe of the slope, which causes lateral expansion and subsequent lowering of the height of maximum flow velocity, increasing basal shear stress and enhancing erosion. The location of the scour field at both the mouth of the Māhia Canyon (where

flows channelled by the canyon system would lose confinement as they enter the Hikurangi Trough) and at the base of a steep break in the slope suggest (b) and (c) are both credible origins of these features.

4.1.2 | Wave Fields

4.1.2.1 | Observations. Beyond the mouth of the Māhia Canyon the Hikurangi Trough slopes $\sim 0.16^\circ$ in a northeast direction and has a stepped appearance due to the presence of a prominent field of asymmetrical waveforms (*sensu* Wynn and Stow 2002), with crests orientated in an NW–SE direction (Figure 5A,B). This Māhia wave field is up to 13 km wide and is bordered by the continental slope to the northwest, the external levee of the Hikurangi Channel to the southeast and the scoured mouth of Māhia Canyon to the west. Wavelengths of the individual bedforms vary from 2.5 to 12.5 km, with wavelength decreasing downslope (Figure 5D). Wave amplitudes are ~ 20 – 30 m and diminish northwards. The downslope faces of the waves are shorter and steeper than those that face upslope (Figure 5D).

4.1.2.2 | Interpretations. The large-scale bedforms on the trough floor are interpreted as sediment waves (*sensu* Wynn and Stow 2002; Symons et al. 2016). Using the classification scheme of Symons et al. (2016), the wavelengths, relief and geometries of these wave fields align with their classification of large-scale sediment waves that were formed by turbidity currents (Wynn and Stow 2002; Orpin 2004; Symons et al. 2016). The crests of the Māhia sediment waves are inferred to have developed normal to the direction of flows debouching from the Māhia Canyon mouth and rotating anticlockwise in a down-flow direction to remain normal to slope gradient (Tek et al. 2022; Figure 5A,B). The reduction in the amplitude and wavelength of the sediment waves towards the north, and gradual transition into a flat plain, indicates a reduction in flow energy northwards due to a dramatic reduction in slope gradient and transition to unconfined flow conditions following its exit from the canyon. The larger scale and asymmetrical morphology of the Māhia wave field differ from those observed elsewhere along the Hikurangi Channel overbank (e.g., Lewis and Pantin 2002; Tek et al. 2022) which typically have wavelengths of > 2 km and amplitudes of > 10 m. Additionally, the Māhia wave field appears to be sourced directly from the Māhia Canyon rather than being formed from overbank flows of the Hikurangi Channel (Tek et al. 2022).

There is a second set of waves with crests orientated in a W–E direction lying to the east of the larger field and within the trough-floor depression north of the Hikurangi Channel bend, hereby referred to as the Tūranganui wave field (Figure 5B, Figure S3). They have a wavelength of ~ 4 km and amplitudes of ~ 20 m, with a width of ~ 6 km. Their morphology is similar to those in the Māhia wave field, with the slope having an asymmetric and stepped appearance overall (Figure 5B, Figure S3). Bathymetric waveforms cease ~ 8 km southwest of Site U1520, with the slope and broader trough transitioning into a gently northeast-sloping plain that extends as far north as the Ruatōria Debris Avalanche (Figure 3A). The trough floor between the two sets of wave fields is topographically

depressed, forming a saddle-like feature that extends northwards from the edge of the bend in the Hikurangi Channel before flattening out alongside the sediment wave fields to the north (Figure 5B).

The Tūranganui wave field exhibits similar morphologic characteristics to the Māhia wave field, although this field is not as geographically expansive. These waves may be formed by a combination of flows being sourced from the Māhia Canyon and subsequently deflected off the sidewalls of the neighbouring Tūranganui Knoll and by flows overspilling the edge of the bend in the Hikurangi Channel directly to the south.

4.1.3 | Hikurangi Channel Bend

4.1.3.1 | Observations. A significant eastward bend occurs in the Hikurangi Channel east of Māhia Canyon, where the channel escapes the Hikurangi Trough to traverse the Hikurangi Plateau (Figures 1, 2 and 5) (Lewis 1994; Lewis, Collot, and Lallemand 1998). Along the 100 km section of the channel to the south, upstream of the bend, cross-sectional profiles reveal a U-shaped channel with a mean width of ~ 3 km (Figure 6B¹). As the channel passes the northern extent of the Māhia Seamount, the eastern flank of the channel loses morphologic definition and the western overbank exhibits a set of obliquely oriented sediment waves with amplitudes of ~ 5 m and wavelengths of ~ 1 km. The channel thalweg then steepens significantly from $\sim 0.014^\circ$ to $\sim 0.38^\circ$ as the channel traverses northward towards the bend (Figure 6B²). A field of enclosed topographic depressions of up to ~ 950 m wide and ~ 15 m deep are present in the channel axis at the base of the steepened thalweg profile (Figures 5 and 6D). TOPAS sub-bottom profiles between D¹ and D² of Figure 6C indicate a distinct acoustic character in this stretch of the channel, with a rugose, uneven surface and no continuous reflections distinguishable (Figure 6C). This contrasts with the section of the channel immediately to the south and north, which is characterised by continuous parallel reflections with smooth morphologies (Figure 6C).

As the channel turns eastwards around the Māhia Seamount (Figure 5) it widens significantly from ~ 3 to ~ 8 km as the channel transitions to a much wider, shallower (~ 75 m), U-shaped cross-sectional profile (Figure 6B¹). This results in a substantial increase in channel aspect ratio, increasing from ~ 30 to ~ 90 . The northeastern, outer flank of the bend has a stepped cross-sectional profile, whilst the southwestern, inner flank is comparatively smooth (Figure 5).

After the bend, the Hikurangi Channel steepens and narrows again to ~ 3 km width, deepening to a channel depth of ~ 150 m, producing a more pronounced U-shaped cross-sectional profile (Figure 6B¹). The sea floor to the north of the eastern branch of the Hikurangi Channel rises by $\sim 0.19^\circ$ ~ 50 m from the edge of the channel, rising against the western flank of the Tūranganui Knoll (Figure 5A,B).

4.1.3.2 | Interpretations. The reduction in channel relief and occurrence of adjacent sediment waves on the basin floor west of Māhia Seamount attest to the loss of channel confinement and overspill of flows (Shumaker et al. 2018). The

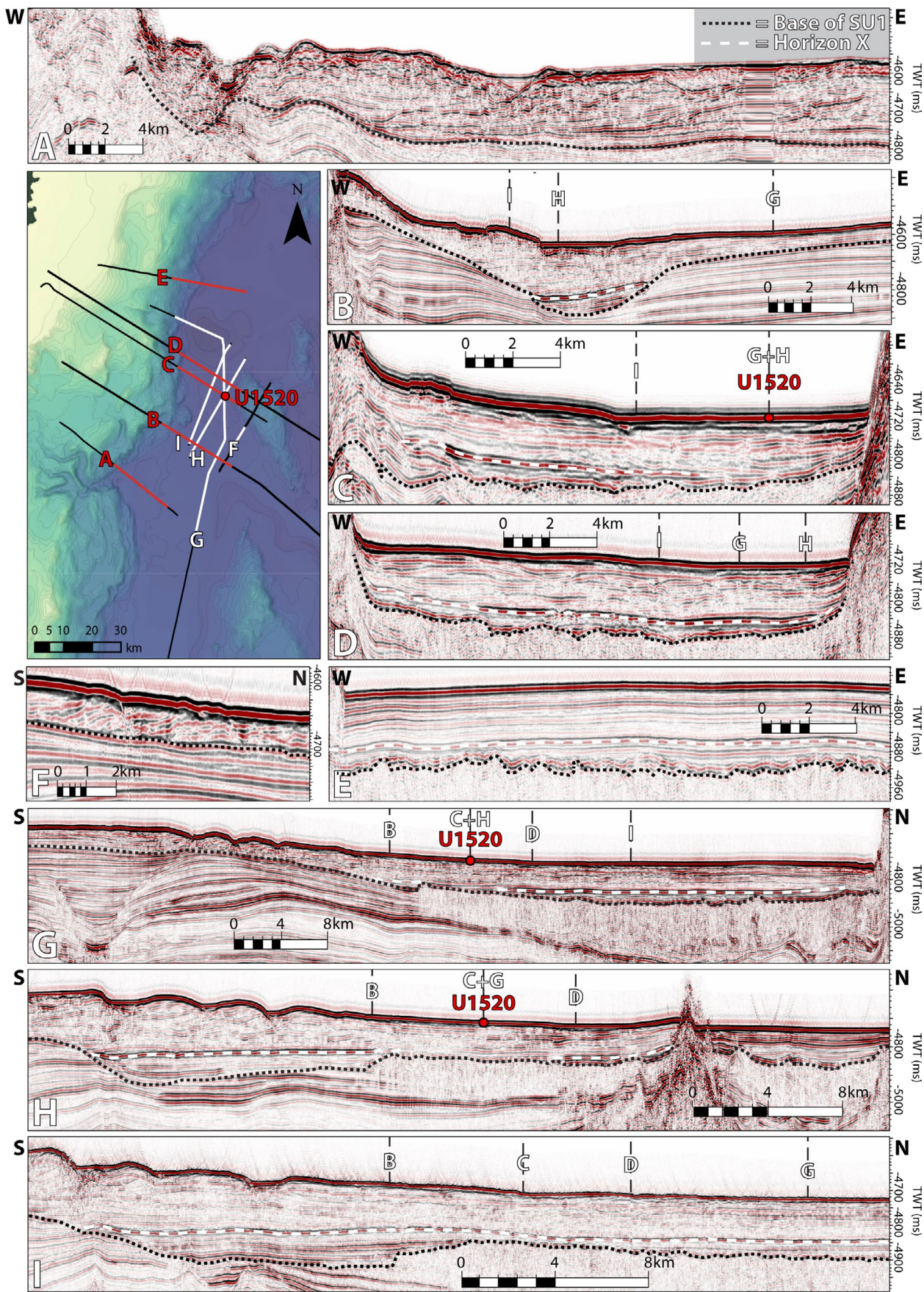


FIGURE 7 | 2D seismic lines (A–I) showing the regional extent of SU1 and Horizon X. Locations of the seismic lines are shown in the inset map. Intersections between the profiles are shown with the respective letters of each profile.

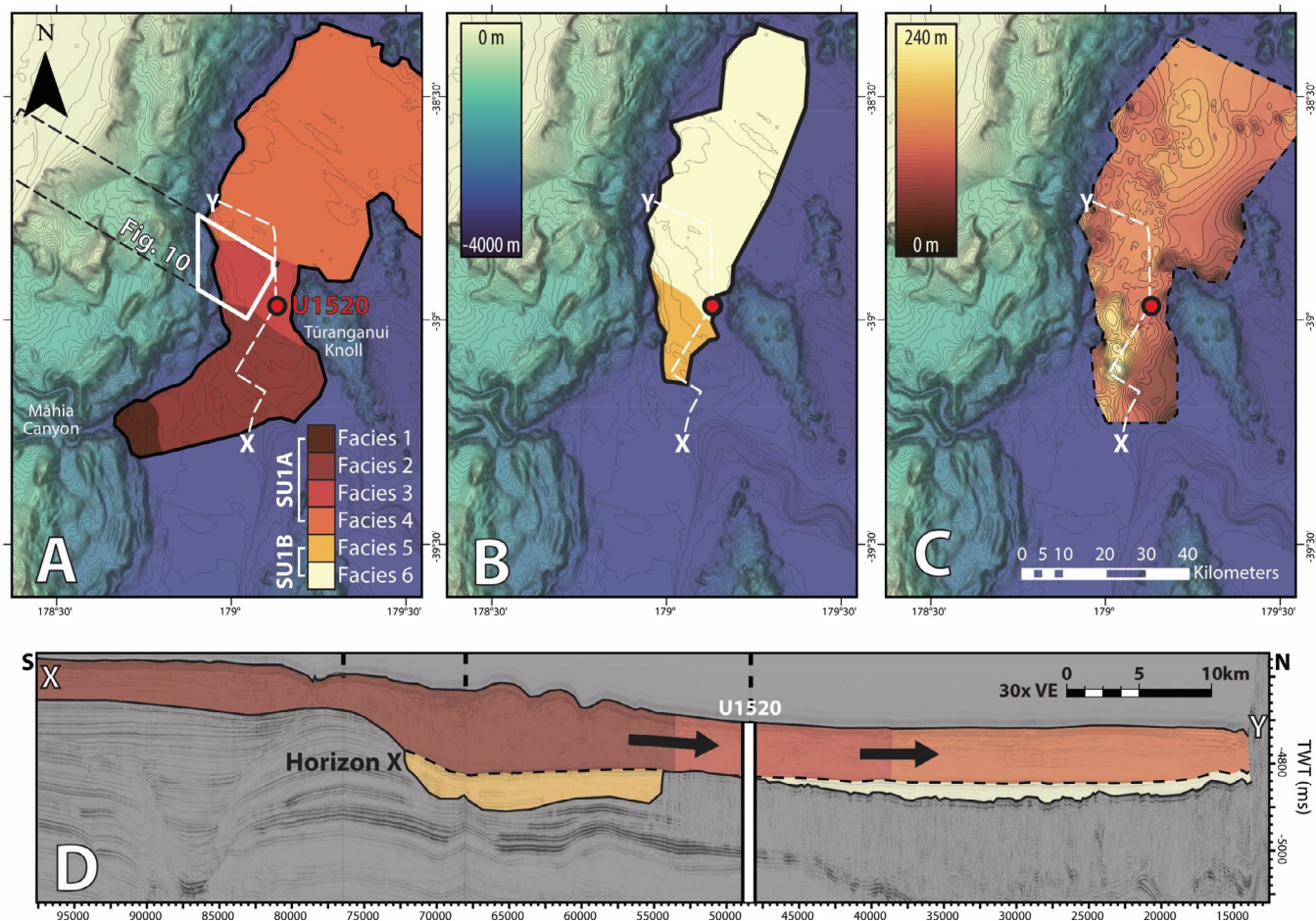


FIGURE 8 | (A, B) Spatial extents of seismic facies identified within SU1. (C) Depth-converted isopach thickness map of SU1. (D) Composite 2D seismic line showing a cross-section of the distribution of facies 2–6. The black arrows indicate a gradual transition between facies 2, 3 and 4.

distinctive acoustic characteristics of the seafloor observed from echo-sounder data through this shallow stretch of the channel indicate that it has been partially infilled by an MTD inferred to have originated from a failure of the western slope of Māhia Seamount (Figure 6C,D). This MTD dammed sediment upstream in the channel and led to a reduced thalweg gradient (Figures 5A and 6B). Further upstream in the southern Hikurangi Channel, MTD emplacement into the Hikurangi Channel has been proposed to induce channel aggradation up to 64 km upstream (Tek et al. 2021; McArthur et al. 2024). The subdued relief of the channel prior to the drop may represent a similar occurrence of channel aggradation (Pope et al. 2022; Figures 5A and 6D). The increased steepness of the Hikurangi Channel thalweg gradient downstream of the MTD is speculated to have led to turbidity current flow acceleration and expansion, which could subsequently contribute to flows overspilling the saddle north of the channel bend and continuing towards Site U1520 (Hiscott, Hall, and Pirmez 1997; Kneller et al. 2016; Wells and Dorrell 2021). Topographic depressions identified along the axis of the channel at the toe of the steepened profile section, west of the Māhia Seamount, are interpreted as erosional scours formed by hydraulic jumps generated by flows reaching a supercritical state in response to the increased channel gradient (Symons et al. 2016).

The increased aspect ratio of the Hikurangi Channel around the bend indicates that its ability to confine turbidity currents is reduced in comparison to the narrower stretches of the channel (Shumaker et al. 2018; Figure 6B). The saddle-like topography on the northern edge of the bend is interpreted as an erosional feature formed by the overspill of northward-flowing turbidity currents (sensu Hiscott, Hall, and Pirmez 1997; Amos et al. 2010). Such overspill would likely be restricted to the fine-grained upper parts of sediment gravity flows, with the coarser and denser lower parts confined to within the walls of the channel continuing east around the bend (Traer et al. 2018; Kelly et al. 2019).

The elevated seafloor on the southern western flank of the Tūranganui Knoll is interpreted as a levee of the Hikurangi Channel (sensu Collinson and Thompson 1982; Figure 5). The positive relief (~50 m) of this levee in relation to the surrounding trough floor is attributed to the western flank of the knoll acting as a dam that has prevented the transport of sediment further northwards/eastwards (Figure 5A,B). Northward-flowing bottom currents redirected along the flanks of the knoll could potentially also contribute to the formation of this feature giving it a mixed turbidite-contourite origin (e.g., Bailey, McArthur, and McCaffrey 2021; Woodhouse et al. 2022; Underwood 2023).

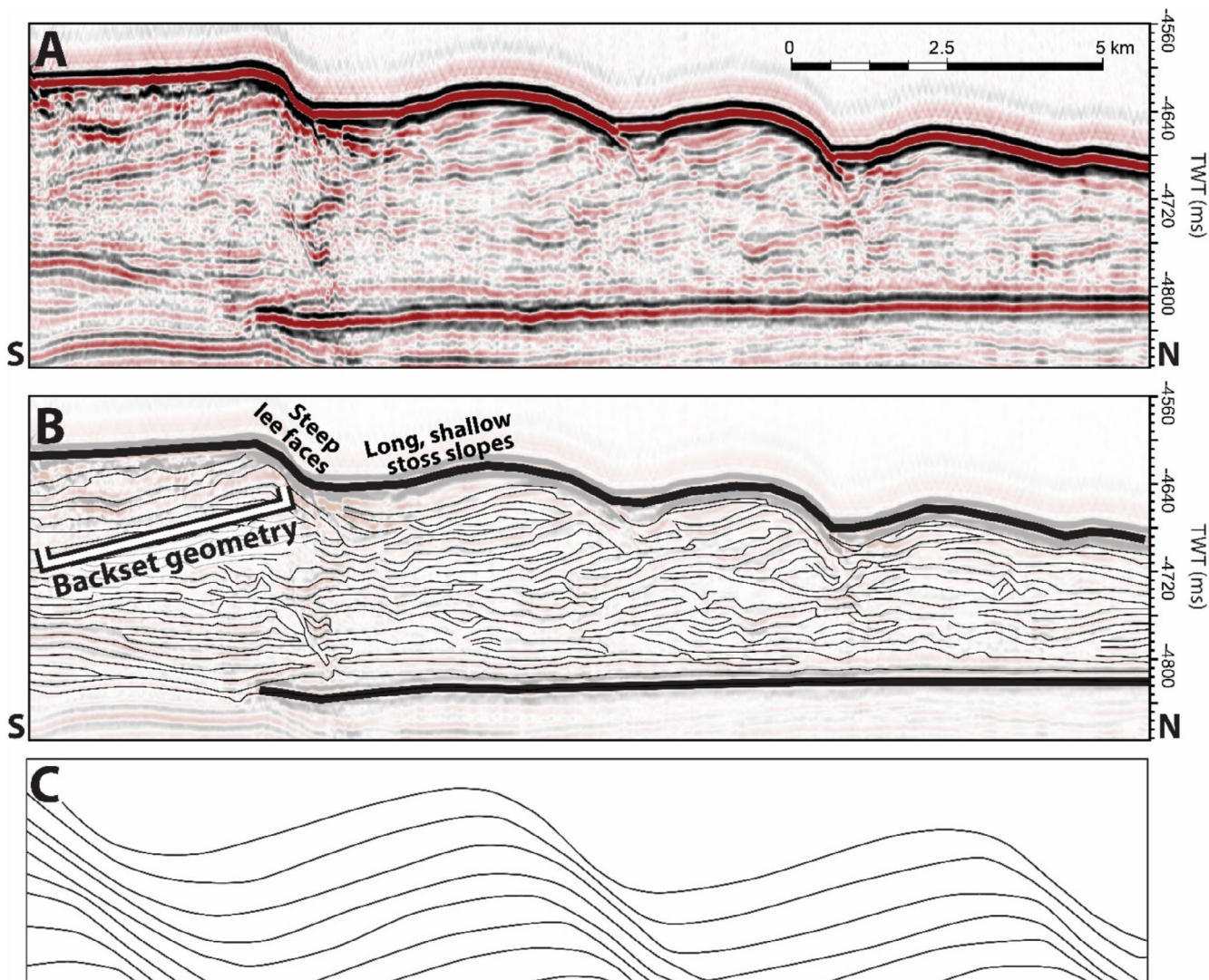


FIGURE 9 | (A) Uninterpreted seismic line TAN1114-04 which overlies the NW-SE orientated sediment wave field to the northwest of the Hikurangi Channel bend. (B) Linework highlighting the interpreted internal geometry of Facies 2. (C) Idealised schematic representation of a strongly aggradational asymmetrical down-slope cyclic step for comparison with (B) (adapted from Cartigny et al. 2011).

4.2 | Seismic Stratigraphy

Below, we analyse and interpret the seismic characteristics of SU1. SU1 is characterised by discontinuous seismic reflections, with moderate-to-high amplitudes and geometries that range from planar to hummocky (Barnes et al. 2019; Figures 3B and 7). Within the extent of the area studied for this publication, SU1 has a mean thickness of 110 m and a maximum thickness of ~240 m (Figure 8C). SU1 is thickest towards the southwestern boundary of the area surveyed, alongside the edge of the continental slope (Figure 8C). SU1 thins towards the southeast where the unit overlies the Hikurangi Channel levee (Figure 7C,G). It also thins towards the western and eastern boundaries of the mapped area where the unit overlies and pinches towards the edges of the continental slope and the Tūranganui Knoll, respectively (Figure 8C).

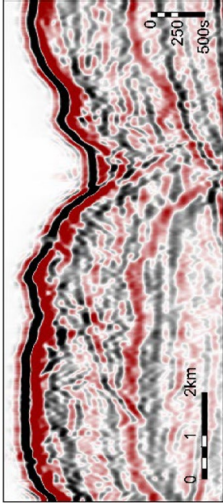
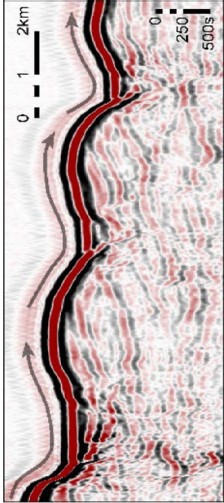
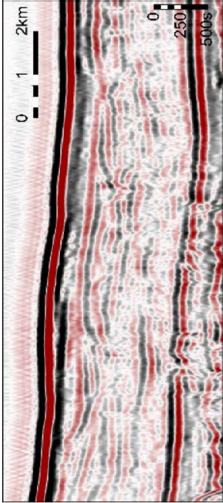
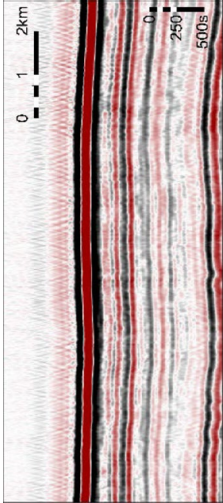
We have further divided SU1 into two subunits and defined six seismic facies that characterise their morphologies and the processes responsible for their formation (Figures 7 and 8). Seismic Unit 1A (SU1A) and Seismic Unit 1B (SU1B) are separated by

a continuous and high-amplitude reflector here referred to as Horizon X, that can be widely traced across the study region, with SU1A being associated with all facies found above this reflector, and SU1B with all that underlies it (Figures 7 and 9D). Correlations with core U1520D indicate that the base of SU1 has an age of ~42 ka, whilst Horizon X aligns approximately with the depth (~95–106 mbsf) of the transition between Marine Isotope Stages (MIS) 3 and 2 (~30 ka) (Woodhouse et al. 2022; Figure 4). The transition between MIS2 and MIS1 (~15 ka) occurs at ~10 mbsf and is typically masked by the impedance contrast of the seafloor within the seismic dataset, hampering the characterisation of geomorphic changes over this time period (Woodhouse et al. 2022; Figure 4).

4.2.1 | Seismic Unit 1A

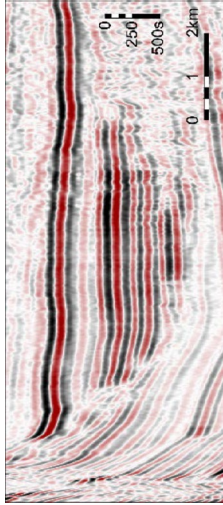
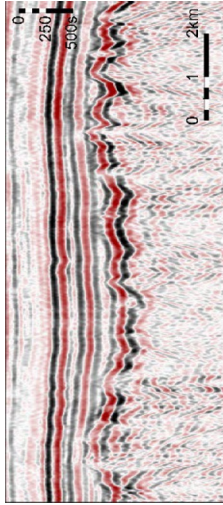
SU1A extends from the seafloor to Horizon X and covers the entirety of the study area, extending southward of the mouth of the Māhia Canyon (Figures 7 and 8). The formation of this subunit was initiated at the start of MIS2 and deposition continues

TABLE 1 | Summary of seismic facies observed within the study region. Horizontal scale bars are in distance (km) and vertical scale bars are in Two Way Time (s).

SU	Facies	Example	Amplitude	Continuity	Configuration	Interpretation
1A	1		Moderate to high	Low	Chaotic and discontinuous reflectors form rounded depressions that frequently truncate underlying depressions	Irregular ovoid erosional scours
	2		Low to moderate	Low to moderate	Varies from sub-parallel to hummocky; characterised by large-scale waveforms that dip inwards towards the direction of the slope (backset)	Sediment waves
	3		Low to moderate	Low to high	Varies from parallel to hummocky; evidence of broad arcuate depressions across the study extent, truncating underlying reflectors	Arcuate erosional scours
	4		Low	High	Parallel; widespread across the entire northern region with no significant variation observed	Basin plain sequence

(Continues)

TABLE 1 | (Continued)

SU	Facies	Example	Amplitude	Continuity	Configuration	Interpretation
	5		High to moderate	Low to high	Parallel reflections that onlap the underlying depression	Sheeted turbidites infilling topographic low
1B	6		Low	High	Conformably overlays underlying features, transitions to parallel when underlying features are buried	Draped sheet of overspilled deposits

through to the present. Six distinct seismic facies can be observed within the subunit.

4.2.1.1 | Facies 1

4.2.1.1.1 | Observations. Facies 1 occurs directly east of the mouth of the Māhia Canyon, directly underlying the scour field depicted in Figure 5 (Figure 8A). This facies is characterised by moderate-to-high amplitude discontinuous reflections with chaotic and discontinuous reflectors forming rounded depressions that frequently truncate underlying depressions (Table 1, Figure 7A).

4.2.1.1.2 | Interpretations. Facies 1 is interpreted as representing infilled erosional scours, similar to the modern expressions of these features observed on the seafloor as depicted in Figure 5, and would be formed by similar processes to those described above (sensu Symons et al. 2016; Pohl et al. 2019).

4.2.1.2 | Facies 2

4.2.1.2.1 | Observations. Facies 2 is found further east of Māhia Canyon and is co-linear with the modern expression of the Māhia sediment wave field (Table 1, Figures 7B,C,G–I, 8 and 9). The facies is characterised by low-to-moderate amplitude, semi-continuous reflections (Table 1, Figure 9). Reflection configuration varies between parallel, sub-parallel and hummocky.

At the regional scale, Facies 2 is defined by large-scale (2–12.5 km wavelengths and 20–30 m amplitudes) asymmetrical waveform features (Figures 5A,B,D, 8G–I and 10). The reflections within the waves are characterised by longer, more gentle slopes dipping towards the south and shorter and steeper slopes dipping to the northeast (Figure 9). The toes of the northward-dipping slopes form curved depressions and have higher amplitudes that subsequently transition into the shallower south-dipping slopes of the succeeding waves.

4.2.1.2.2 | Interpretations. The asymmetric morphology and backset internal structures of the waveforms are consistent with descriptions of asymmetrical down-slope cyclic steps formed by turbidity currents (sensu Cartigny et al. 2011; Cartigny et al. 2014; Slooman and Cartigny 2020). The long and shallow southward-dipping slopes of the sediment waves are interpreted as representing the stoss side of each wave, whilst the steeper northward-dipping slopes represent the lee faces (Figure 9). The southerly-dipping internal reflections identified within each bedform are interpreted as being indicative of backset deposition along the stoss slopes of each wave. Large-scale sediment waves in unconfined settings have been associated with cyclic steps in other localities, resulting in steps that are more prone to aggradation (and subsequently increased waveform size) as opposed to erosion in confined settings (Cartigny et al. 2011; Symons et al. 2016).

4.2.1.3 | Facies 3

4.2.1.3.1 | Observations. Facies 3 is characterised by low to moderate amplitude, semi-continuous to continuous reflections

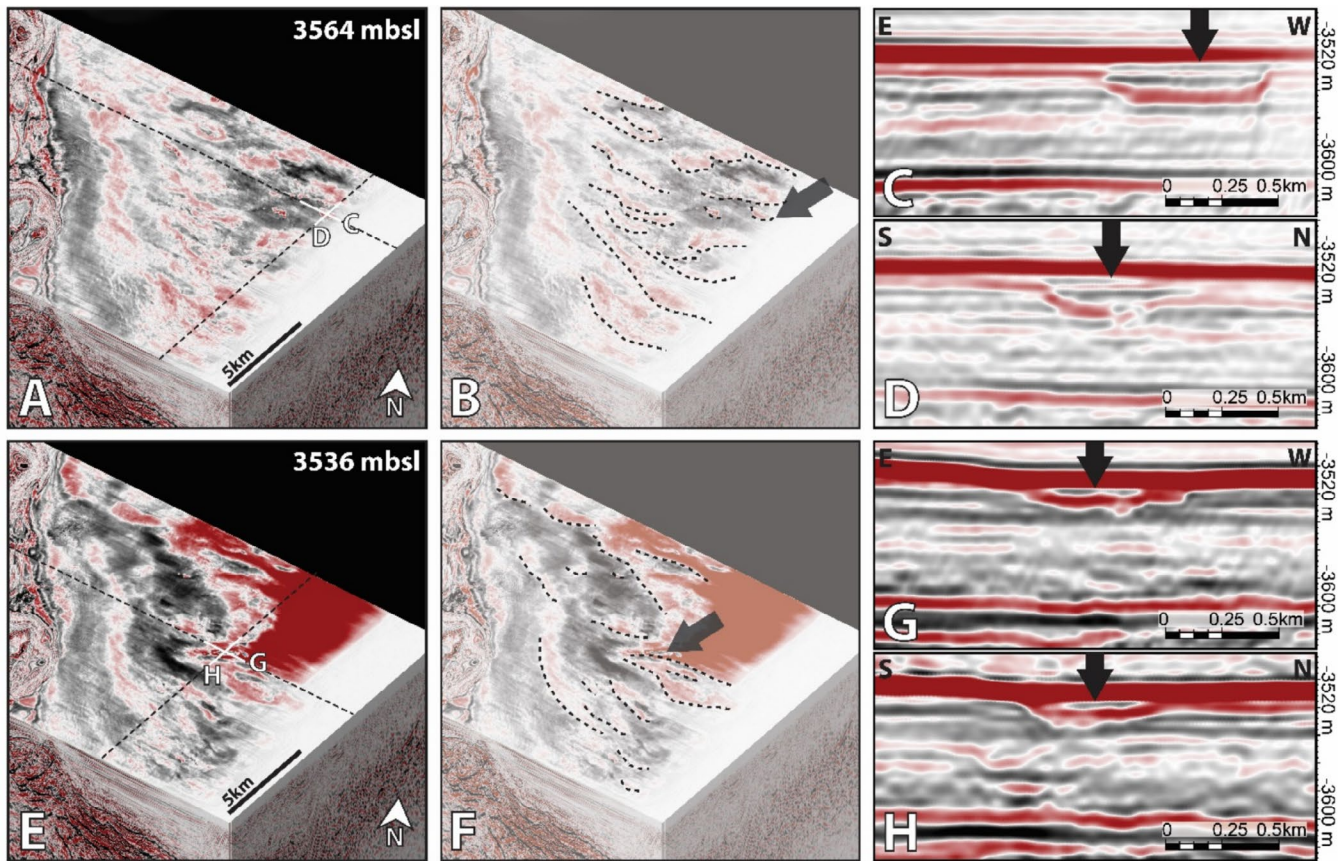


FIGURE 10 | (A) Uninterpreted 3D seismic surface displaying scours at a depth of 3564 mbsl. (B) Interpreted 3D seismic surface of (A), with dashed lines highlighting scours and an arrow showing the location of scour shown in (C) and (D). (C) SW–NE by-line of the 3D seismic cube showing a scour in (A). (D) NW–SE by-line of the 3D seismic cube showing a scour in (A). (E) Uninterpreted 3D seismic surface displaying scours at a depth of 3536 mbsl. (F) Interpreted 3D seismic surface of (E), with dashed lines highlighting scours and an arrow showing the location of scour shown in (G) and (H). (G) SW–NE by-line of the 3D seismic cube showing a scour in (E). (H) NW–SE by-line of the 3D seismic cube showing a scour in (E).

(Table 1, Figures 7D,E,G–I and 10). This facies occurs downslope of Facies 2 and is identified in the stretch of the trough constrained between the continental slope and by Tūranganui Knoll (Figure 8A,D). The facies gradually transitions into Facies 4 to the north as the trough opens into a wide and unconfined plain.

Many reflections within this facies appear to incise and truncate underlying reflections (Figures 7D,E and 10). When viewed in the NZ3D seismic cube, these reflections laterally extend across the width of the data volume in concentric, elliptical shapes, forming large-scale low amplitude bedforms with depressed topography in comparison to their surrounding reflections (Figure 10).

4.2.1.3.2 | Interpretations. The large-scale arcuate bedforms that define this region of the trough are interpreted as buried scours. Such features are not evident in the modern expression of the seafloor, and they do not share the same circular geometry observed in the modern examples of erosional scours observed at the mouth of the Māhia Canyon and within Facies 1 (Figures 5C and 10). The 2D expression of these features could be interpreted rather as buried channels, but the 3D data makes it clear that they are laterally continuous features in an E–W orientation (Figure 10). Their origin could be related to the ‘flow relaxation’ process described above (Pohl et al. 2019). The western levee of the Hikurangi Channel

could serve to partially confine flows exiting the Māhia Canyon; as these flows continue northwards of the channel and away from the levee into a comparatively flat and featureless plain, they laterally expand and the associated lowering of the height of maximum velocity increases their ability to form erosive features such as scours (Pohl et al. 2019; Hodgson, Peakall, and Maier 2022). The massive sand beds (55–90 mbsf) observed at Site U1520 (Figure 4) could be associated with these scours. The absence of these features on the modern seafloor within the mapped extent of Facies 3 suggests that they were formed during MIS2; at Site U1520, MIS1 is represented by a thin veneer of just ~10 m thickness (Woodhouse et al. 2022).

4.2.1.4 | Facies 4

4.2.1.4.1 | Observations. Facies 4 occurs in SU1A to the north of Tūranganui Knoll and drapes the entirety of the mapped extent of the northern plain (Figure 8A,D). The flat, planar and continuous reflections of this facies are configured in parallel and have sheetlike external geometries (Table 1, Figure 7E,G–I).

4.2.1.4.2 | Interpretations. This facies is formed by laterally extensive and lower velocity flows that lack the energy to form erosive features and instead result in large-scale

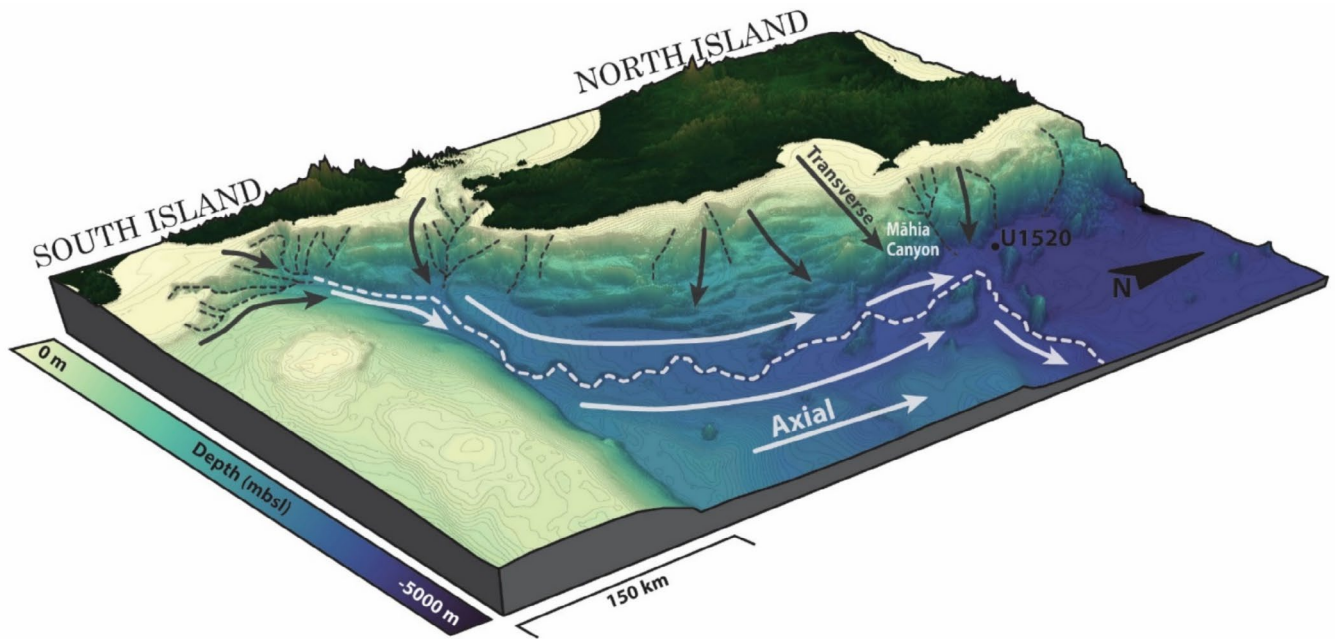


FIGURE 11 | 3D map highlighting the various transverse and axial sediment transport systems operating along the HSM and their relation to Site U1520. Dashed black lines show transverse sediment pathways along the margin, and the white dashed line shows the path of the axial Hikurangi Channel. See Figure 2 for names of major canyon systems in this region.

tabular aggradation, interpreted as representing basin-plain deposits (*sensu* Mutti 1977). Bathymetry and seismic coverage of the region show that the surface elevation of this basin-plain is ~50 m higher than the seafloor east of the seamounts, indicating that distal gravity flow deposition is controlled and restricted by these topographic obstacles (Lewis, Collot, and Lalle 1998; Figure 5A). An absence of seismic coverage to the northeast makes it difficult to determine the full spatial extent of this facies (Figure 3).

4.2.2 | Seismic Unit 1B

SU1B is found beneath Horizon X (Figures 7 and 8D). This unit tapers towards the continental slope to the west and the slope of the Tūranganui Knoll to the east. Correlation of the borehole tie with the U1520D age-depth model indicates this subunit was deposited during MIS3 (Woodhouse et al. 2022). It is comprised of two dominant seismic facies (Facies 5 and 6).

4.2.2.1 | Facies 5

4.2.2.1.1 | Observations. Facies 5 is characterised by moderate to high amplitude reflections that are highly continuous. Their configuration is largely parallel and sheet-like in nature (Table 1, Figure 7B,G-I). The spatial extent of Facies 5 within SU1B is initially almost entirely restricted to within a depression towards the south of the study area, adjacent to the continental margin but extends further northwards as it accumulates up to Horizon X (Figure 7B,D).

4.2.2.1.2 | Interpretations. This facies is interpreted to be formed by unconfined, laterally extensive sediment gravity flows and hemipelagic settling. Minimal erosion is inferred, resulting

in the characteristic tabular and undisturbed geometry composed of well-bedded turbidites and hemipelagites (Mutti 1977; Pilkey, Bush, and Rodriguez 1988; Shanmugam 1988; Talling, Amy, and Wynn 2007; Talling et al. 2012; Clare, Talling, and Hunt 2015). The elongated depression that Facies 5 infills in SU1A may represent an N-S orientated trough that was confined by the emplacement of the RMTD (Lewis, Collot, and Lalle 1998). This trough may extend as far southwest as the mouth of the Māhia Canyon, but further work is required to confirm this. Horizon X marks the upper surface of the infilled trough; this horizon potentially represents a change in lithology associated with a shift in depositional conditions; observations of core material from Site U1520 align with this interpretation, with the occurrence of massive sand beds only occurring above Horizon X (Barnes et al. 2019; Woodhouse et al. 2022; Figure 4). This shift could be caused by the transition from deposition within the trough to an unconfined basin-floor setting (Figure 8D).

4.2.2.2 | Facies 6

4.2.2.2.1 | Observations. Facies 6 is characterised by low amplitude, continuous reflections (Table 1, Figure 7F-I). Their configuration conformably overlies the irregular underlying surface of SU2 (Figures 7F and 8D). The elevated surface and rugose surface of SU2 act as a morphologic barrier for much of this unit, preventing it from covering the full extent of the mapped region (Figure 8B).

4.2.2.2.2 | Interpretations. Facies 6 is formed as a result of deposition from flows that overspilled the infilled trough described above, and subsequently lost confinement, leading to widespread deposition of sheet-like structures (e.g., Hiscott, Hall, and Pirmez 1997). The flows that formed these facies were controlled by the surface morphology of the RMTD, resulting in

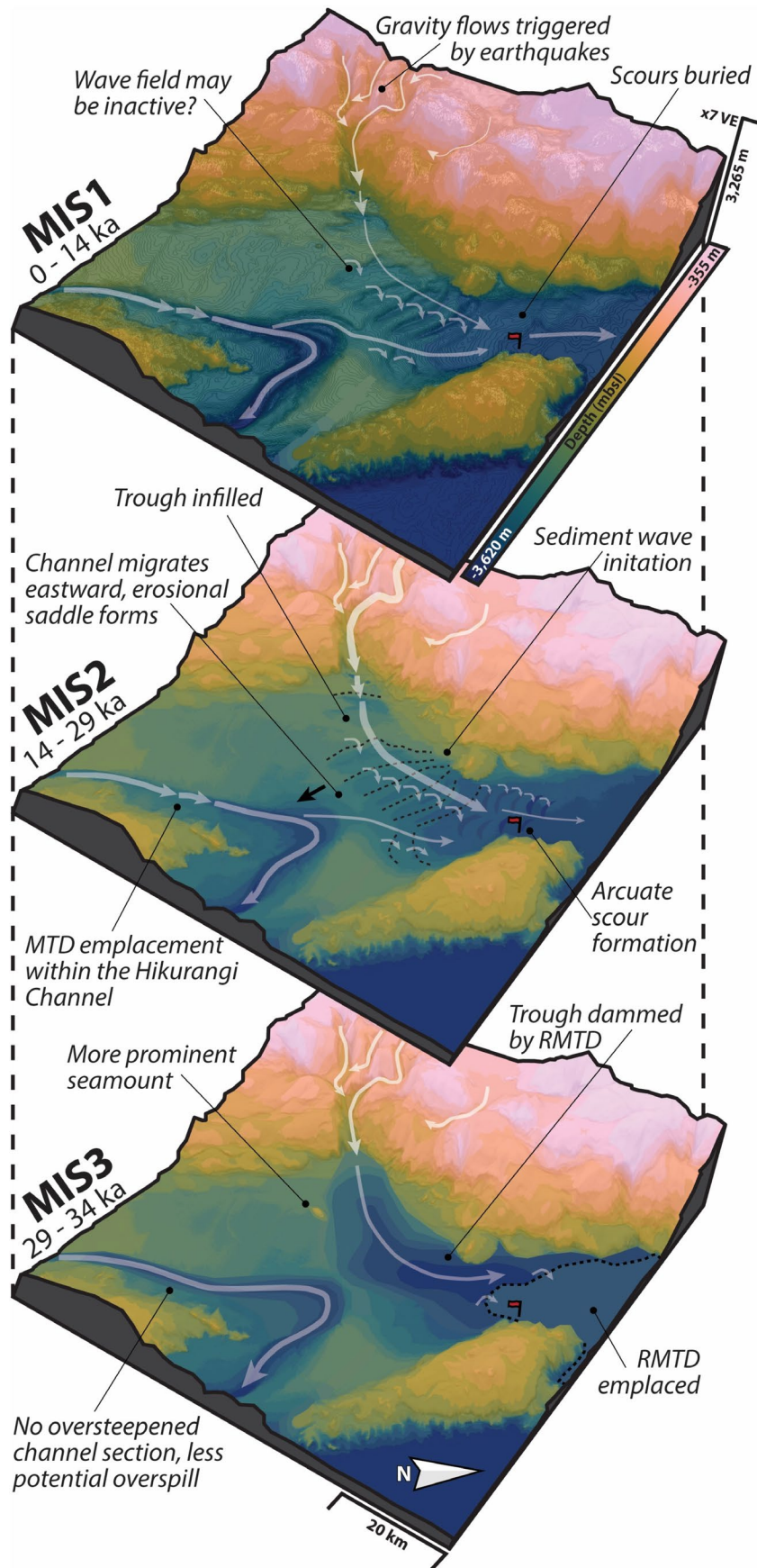


FIGURE 12 | Schematics representation showing flow pathways in the study region and the changes in the geomorphological characteristics of the study region between MIS3, MIS2 and MIS1. MTD = Mass Transport Deposit, RMTD = Ruatōria Mass Transport Deposit. The red flag shows the location of Site U1520 and the dashed black line shows the extent of the RMTD.

the deposition of reflections that weakly conform to the underlying surface. Successive depositional events would have gradually infilled the initially irregular surface of RMTD as it transitioned to the much flatter and more tabular geometry of Facies 4.

5 | Discussion

5.1 | Sediment Delivery Pathways to the Northern Hikurangi Trough

Analysis of both the surface and subsurface geomorphology of the study region indicate that there are two dominant pathways for sedimentary gravity over the last 42 ka forming SU1: (a) transverse flows directly exiting the Māhia Canyon and (b) axial flows overspilling the bend in the Hikurangi Channel (Figures 11 and 12).

Sediment gravity flows sourced from the Māhia Canyon would likely be composed primarily of North Island-derived sediments that originate close to the edge of the continental shelf, or within the canyons themselves, and would flow down a steep (2.7° – 3.5°) and sinuous network of canyons that deeply incise the continental slope (Figure 11; Orpin 2004; Pedley et al. 2010; Poudroux et al. 2012). This is supported by the identification of benthic foraminifera in core material from Site U1520 that are indicative of sedimentary input from paleo-water depths of 0–1000 mbsl across SU1, far shallower than the actual water depth at Site U1520 of 3520 mbsl (Crundwell and Woodhouse 2022; Woodhouse et al. 2022). Such flows were likely to be highly erosive, with canyon slopes exceeding the critical threshold (0.57°) required for flows to become supercritical and are responsible for the formation of large-scale erosional scours observed on the trough floor (Sequeiros 2012; Postma and Cartigny 2014; Figure 5). The orientation of the Māhia wave field further implies a strong influence of transverse flows to the north (Figure 5).

In contrast to the largely erosive and high-energy flows of the Māhia Canyon, the Hikurangi Channel is interpreted as a constructional, aggradational channel-levee system sourced primarily from the South Island (Lewis, Collot, and Lalle 1998; McArthur and Tek 2021; Tek et al. 2022; Maier et al. 2024). However, there are sections where steepened gradients or constrictions have caused accelerated and erosional flows. For example, the emplacement of an MTD in the channel, originating from the side of the Māhia Seamount, would have driven the localised steepening (Figure 6B). This would have allowed flows from the south to have accelerated down local slopes, become more turbulent and potentially supercritical (as indicated by the formation of erosive scours at the toe of the steepened section of the thalweg) in this location. This flow acceleration could facilitate the overspill of flows over the northward edge of the bend, where the formation of a topographic saddle implies an erosive flow regime driven by flow overspill (Hiscott, Hall, and Pirmez 1997; Figure 5). Similar processes have been observed further upstream in the channel, where knickpoints have migrated upstream with the result of shifting sediment from up-to-downstream (i.e., ‘cut-and-fill’) and demonstrating how steepened sections of the channel can influence flow behaviour (Tek et al. 2021). The existence and highly positive relief of the levee against the southern flank of the Tūranganui Knoll

provides further evidence of the occurrence of flow overspill at this location.

Whilst several other pathways along the continental slope, particularly to the north, could also contribute to regional sediment delivery, their reduced morphologic expressions and directions in opposition to the regional slope suggest that they do not contribute significant volumes of sediment to the area in comparison to the Māhia and Hikurangi systems (Figures 3 and 12). As discussed in Poudroux et al. (2012), the Paritu Channel is inferred to primarily feed sediment to the Paritu Trough and Lower Paritu Basin rather than to the Hikurangi Trough. Regional bathymetry also exerts a strong influence on the distribution of sediment delivery; the Tūranganui Knoll for example exhibits a significant ‘damming’ effect, resulting in markedly lower sediment accumulation to the east of the knoll in comparison to the west (Figure 5). These features are also hypothesised to influence the long-term evolution of the Hikurangi Channel, with the bend potentially forming in response to the northern reaches of the margin being blocked by the presence of seamounts (Lewis, Collot, and Lalle 1998).

5.2 | Stratigraphic Evolution of the Northern Hikurangi Trough

The seismic and sub-bottom profile data provide evidence of how the geomorphology of the northern Hikurangi Trough has evolved over the last 42 ka (Woodhouse et al. 2022). The geomorphic and sedimentological character of the study region has undergone significant changes over this period, particularly in response to glacial eustasy. Here we discuss how the shifting environmental conditions between MIS3 (42–30 ka), MIS2 (30–15 ka) and MIS1 (15–0 ka) have influenced the behaviour of transverse and axial sediment pathways that are responsible for sourcing the sedimentary deposits that form SU1 (Woodhouse et al. 2022; Figure 12).

5.3 | MIS3

The initiation of the development of SU1B at 42 ka would have occurred soon after the emplacement of the Ruatōria Debris Avalanche, and the associated RMTD that underlies much of the northern extent of the study region (Barnes et al. 2019; Woodhouse et al. 2022). The RMTD is inferred to have dammed an elongated trough that extends northwards from the mouth of the Māhia Canyon and underlies the modern expression of the Māhia wave field (Figure 12). Initial deposition of SU1A would have been confined to within this trough (Facies 4) and overlying the top surface of the RMTD to the north (Facies 5), with flows ponding in topographic lows and overspilling to drape over the wider surface. The orientation of this trough, and the distribution of the facies associated with it, implies that flows sourced from the transverse sediment pathway of the Māhia Canyon would have been responsible for the formation of this unit. Prior to the emplacement of the RMTD and the resultant changes in the regional topography, flows sourced from the Māhia Canyon may have largely bypassed this area of the trough, and instead continued to the north (Stevenson et al. 2015). The topography

immediately underlying the depression is associated with the levees of buried channels, possibly representing the prior expression of the Hikurangi Channel (Figures 7 and 9). Horizon X coincides with the start of MIS2 (~30 ka), and the 'top' of the infilled trough.

The rugose appearance and the absence of any evident overlying reflections atop the MTD within the Hikurangi Channel west of Māhia Seamount (Figure 6) suggest that this feature was emplaced relatively recently, and we speculate here that it was not in place during MIS3 (Figure 12). As a result, the Hikurangi Channel would have been more deeply incised and had a gentler slope leading up to the bend, which would confine flows and limit their ability to accelerate as they approach the bend and subsequently overspill, potentially reducing the influence of axial sediment transport to the northern Hikurangi Trough during this period.

5.4 | MIS2

At the regional scale, above Horizon X, MIS2 marked the initiation of the development of SU1A, including the formation of the Māhia wave field, and the large-scale arcuate scours further to the north (Figures 7, 10 and 11). The initiation of the wave field could have been related to pre-existing irregularities on the seafloor, but there is no indication of such features existing in the seismic stratigraphy, and experimental and numerical models have demonstrated that sustained sediment gravity flows can produce these bedforms without this precondition (Cattaneo et al. 2004; Spinewine et al. 2009; Kostic and Parker 2006; Symons et al. 2016). Bathymetric and seismic coverage suggests that the Māhia wave field was formed independently of the Hikurangi Channel with no direct link between the two features evident, but the levee of the channel could have acted to partially confine Māhia-derived flows between it and the edge of the continental slope. Previous authors have suggested that the Māhia Canyon may contribute flows to the Hikurangi Channel (Lewis, Collot, and Lalle 1998; Pedley et al. 2010; Poudroux et al. 2012). However, the propagation and orientation of the Māhia wave field imply that sediment gravity flows from the canyon largely do not converge with the Hikurangi Channel and were instead directed northeast along the edge of the continental slope. This could possibly be due to the influence of centrifugal and southern hemisphere Coriolis forces directing flows towards the continental slope, alongside the influence of the regional bathymetric gradient dipping towards the north (Carter and Carter 1988; Peakall et al. 2012).

Woodhouse et al. (2022) demonstrated that at Site U1520, Horizon X marks the onset of multi-m thick sands (55–90 mbsf, Figure 4), and the depositional rate in MIS2 was substantially higher (~2.5–20 m/ka, ~33-year recurrence interval (RI) of gravity flow events) during this glacial period in comparison to the MIS3 (0.3–1.7 m/ka, ~131-year RI) and the present interglacial MIS1 (0.5–1.3 m/ka, ~237-year RI). The coincidence of this significant increase in sedimentation rate with the initiation of large-scale sedimentary features (in the form of scours and asymmetric cyclic steps) suggests that these changing environmental conditions caused a significant shift in the geomorphologic expression of the trough floor in the study region. The

sediment waves in the Māhia wave field, described here in detail for the first time, are comparable to the largest recorded in the world with wavelengths of up to 12.5 km and amplitudes of up to 30 m (Wynn and Stow 2002; Symons et al. 2016). The maximum wavelengths recorded here exceed the hypothesised maximum wavelength of 7.2 km for large-scale sediment waves presented in Symons et al. (2016) and may demonstrate the potential for sediment gravity flows to create features of even greater size than previously recognised. The large-scale bedforms observed within the SU1A are almost exclusively orientated within the direction of flows inferred to have exited from the mouth of the Māhia Canyon (Figures 7 and 12). The thick (up to 6.4 m), sandy beds at Site U1520 (Figure 4) display a potential association with the arcuate scours of Facies 3 and could have resulted from the deposition of coarser and sandier material within topographic lows (Talling, Amy, and Wynn 2007). Woodhouse et al. (2022) speculate that there is a sea-level threshold (-110 ± 10 m below modern sea level), at which the Māhia Canyon 'activates', and sediment flux markedly increases as the head of the canyon directly connects to sediment sourced from the continental shelf.

The thick, sandy beds at Site U1520 are unlikely to be sourced from the dilute upper parts of flows that would have overspilled the bend of the Hikurangi Channel, especially in the absence of any evidence of breaching and crevassing. The erosional nature of the Hikurangi channel as it redirects around the bend indicates that axially transported sediment is predominantly transported east (Underwood and Karig 1980; McArthur and Tek 2021). However, there are still large volumes of fine sediment within the U1520 record which could potentially be associated with axial sediment delivery via overspill of the Hikurangi Channel. The emplacement of the MTD to the west of the Māhia Seamount, and the associated ramping effect, may have occurred during MIS2 and facilitated increased overspill of the bend (Figure 12). More detailed sedimentological studies are required to assess the provenance of these sediments.

5.5 | MIS1

MIS1 is characterised by lower sediment fluxes to the northern Hikurangi Trough, as indicated by significantly lower sedimentation rates (0.5–1.3 m/ka) than in MIS2 (~2.5–20 m/ka) at Site U1520 (Woodhouse et al. 2022; Figure 4). The topographic expression of the Māhia wave field is still well-defined, but without acquiring additional data, such as from sediment cores or active flow monitoring, it is not possible to say whether they are active or relict features. There is no evidence of any large-scale arcuate scours on the modern seafloor in the vicinity of Site U1520. Instead, this area is defined by a subdued trough floor setting with no significant geomorphic features identified. This may indicate that flows are dominantly dispersive and depositional rather than erosive during the Holocene. Resolution limitations of both bathymetric and seismic datasets may mask the potential occurrence of smaller-scale bedforms. Acquisition of higher-resolution subsurface profiles would assist in the characterisation of the seafloor during this upper interval.

The influence of transverse sediment delivery via the Māhia Canyon during the Holocene is likely diminished in the region if the sea-level threshold hypothesis of Woodhouse et al. (2022)

is correct. This could explain the absence of scours north of the wave field in the modern setting. Numerous cores have been acquired from and in the vicinity of the Hikurangi Channel following the 2016 Kaikōura earthquake, with deposits from this event reaching as far as the edge of the Hikurangi Plateau (Howarth et al. 2021; Maier et al. 2024; McDonald et al. 2024). This proves that the Hikurangi Channel is an active conduit of sediment gravity flows in the modern setting, and as outlined in this publication may continue to be a source of sediments directed towards the northern Hikurangi Trough. Whilst individual canyon systems, such as the Māhia Canyon, may be relatively inactive during sea-level highstands, the wider axial system may be comparatively active as it is sourced from multiple transverse systems along the HSM of which some may continue to connect to sediment sources along the continental shelf (Lewis and Barnes 1999; Howarth et al. 2021; Maier et al. 2024). Sweet and Blum (2016) found that sand-sized material is funnelled into deep marine settings when canyon heads are within 1–5 km of river mouths of longshore-drift cells, which is the case for several canyon systems (including the Kaikōura Canyon) to the south, but is not for the Māhia Canyon, and would explain how the Hikurangi can behave as a sustained system during the Holocene highstand. However, Sweet and Blum (2016) also found that clay- and silt-sized particles can persist in a system if a canyon head is within ~40 km of the shoreline (as is the case for the Māhia Canyon), so it is likely that whilst sediment flux to the canyon is diminished during highstands, it is not an entirely relict system. Underwood (2023) identified an unusually broad continuum of clay compositions within U1520 hypothesised to be invoked by transport from both transverse and axial sediment pathways, alongside variable amounts of mixing amongst suspensions from diverse sources and fluctuations in suspension durations within nepheloid layers. Detailed sediment provenance studies to disentangle the sources of the sediments that compose the U1520 sequence would help answer these outstanding questions, as would the acquisition of additional, longer sediment cores from the northern trough and the Hikurangi Channel.

5.6 | Transverse Versus Axial Sedimentary Transport Systems

This study highlights the importance of considering the influence of transverse versus axial sediment routing into the trough and how the sediment routings can be affected by tectonic and climatic forcing. Turbidite-dominated sedimentary records from along the Hikurangi Trough have proven to be useful proxies for understanding the paleoseismic (e.g., Poudroux, Proust, and Lamarche 2014; Howarth et al. 2021; Pizer et al. 2024) and paleoclimatic (e.g., Woodhouse et al. 2022; McDonald et al. 2024) history of the HSM. The U1520 sediment record presents an opportunity to expand these studies deeper in time, beyond what can be accomplished with short (>25 m) sediment cores, most of which only record sedimentation during the Holocene. However, future studies will have to consider the dramatic shift in sediment flux to the northern trough during sea level lowstands, with sedimentation rates driven by ‘activation’ of the Māhia Canyon far exceeding those seen in highstands (Woodhouse et al. 2022; Figure 4). Paleoseismic studies of the HSM already contend with the challenges of sourcing

the origins of co-seismic turbidites, with individual earthquake events potentially triggering sediment gravity flows in multiple canyons that all feed into a singular axial system (Howarth et al. 2021). Such challenges would be amplified at Site U1520 due to the ambiguity in distinguishing whether beds are sourced from axial or transverse flows. Analyses of the longer and older record within the U1520 sequence would be further complicated by the increased uncertainty in the triggering mechanisms of the sediment gravity flows, with the significant increase in event frequency during the LGM suggesting that earthquakes alone are unlikely to be the only trigger (Poudroux, Proust, and Lamarche 2014; Woodhouse et al. 2022).

Furthermore, the high-resolution age-depth model acquired from Unit I of the U1520 sequence provides a unique opportunity to assess the evolution of sediment-rich trench sequences in active margin settings. As stated by Woodhouse et al. (2022), many prior studies of long-term sediment records from convergent margins do not capture the high variability of climatic-eustatic cyclicity at the 10^3 to 10^4 -year-scale due to the limitations of age-depth control methods typically employed over 10^5 to 10^6 -year timeframes. The integration of high-resolution age-depth control with regional bathymetric and seismic datasets here provides an example of how variable rates of transverse and axial sediment transport in response to eustatic sea level changes has exerted significant influence on both overall sediment flux and geomorphic characteristics of the northern Hikurangi Trough. The modern geomorphic expression of the region, dominated by large scale sediment waves, primarily reflects sediment routing conditions during the sea level lowstand of the LGM. Other active margins have displayed similar strong responses to increased sediment flux during the LGM. For example, Völker et al. (2013) found that the distribution of sediment in the Chile Trench is best explained by phases of high sediment flux combined with axial transport during sea level lowstands, and lower sediment flux during sea level highstands in which local transverse sediment transport is dominant. In contrast, Bourget et al. (2010) show that the Makran subduction zone exhibits high rates of sediment flux in both sea level lowstands and highstands. During the highstand sedimentation within Makran Trench is associated with occasional mass flushing of mud-rich, river-derived sediments accumulated along the shelf edge and upper slope, as opposed to more frequent, smaller events funnelled through the direct connection of submarine canyons with river systems during lowstands (Bourget et al. 2010). The combination of both flow regimes results in consistent sediment supply to the axial channel on the trough floor regardless of sea level (Bourget et al. 2010). Similar dynamics could occur in the Hikurangi Trough, with the axial Hikurangi Channel staying comparatively active during the highstand fed by submarine canyons, such as the Kaikōura Canyon, that maintain direct connections to terrestrial river systems during sea level highstands (Lewis and Barnes 1999), in contrast to the transverse Māhia Canyon during lowstands. These examples highlight the necessity of nuanced consideration of how axial and transverse sediment transport regimes function in different regions in response to changing environmental conditions. Similar relationships as noted here may be unveiled through the acquisition of higher-resolution age-depth models for analogous settings where existing datasets may lack the resolution to identify these relationships.

6 | Conclusions

This study utilised the integration of bathymetry, 2D and 3D seismic data with sedimentological data from Site U1520D to investigate the geomorphic characteristics of SU1, revealing the complex interplay between transverse and axial sediment transport in shaping the northern HSM region. The evidence suggests that transverse sediment delivery has been the dominant driver of sediment accumulation in this region over the last 42 ka, particularly during MIS2, with the Māhia Canyon playing a key role in this process. Large-scale bedforms, including erosional scours and sediment waves—the latter being some of the largest recorded—are attributed to sediment flows originating from the Māhia Canyon, highlighting its significant influence on the region. Whilst axial sediment transport via the Hikurangi Channel has also contributed to sediment delivery, particularly through the formation of an erosional saddle on the northern channel edge, its impact is secondary to that of transverse flows. This study underscores the importance of considering the dominant transverse sedimentation with lesser axial contributions when interpreting sedimentological and paleoclimate records from U1520D in the Hikurangi Trough. The results of this study, and findings from similar settings, emphasise the need for a nuanced understanding of both transverse and axial systems in trench-filling processes, as well as the variability of their responses to glacial eustasy.

Acknowledgements

We acknowledge and thank the National Institute of Water and Atmospheric Research (NIWA) for data access. Thank you to Katie Maier and Scott Nodder of NIWA for the invitation to join the TAN2207 voyage and the subsequent acquisition of echo-sounder data that was utilised in this project. We also acknowledge and thank the International Ocean Discovery Program (IODP) for their work during Expeditions 372/375 and for providing samples and data that supported this study. We thank SLB for the generous academic licensing of the Petrel 2020 software suite. Funding for this project is from a University of Auckland Doctoral Scholarship and the Marsden Fund of the Royal Society Te Apārangi (PI Lorna Strachan, 20-UOA-099). D. Gamboa thanks the financial support to CESAM by the Portuguese Fundação para a Ciência e a Tecnologia (FCT) I.P./MCTES through national funds (PIDDAC) UIDP/50017/2020, UIDB/50017/2020 and LA/P/0094/2020. We thank Meg Baker, Cornel Olariu, Mads Huuse and an anonymous reviewer for their thoughtful and constructive reviews of the manuscript. Open access publishing facilitated by The University of Auckland, as part of the Wiley - The University of Auckland agreement via the Council of Australian University Librarians.

Conflicts of Interest

The authors declare no conflicts of interest.

Data Availability Statement

The data that support the findings of this study are available from the corresponding author upon reasonable request.

Peer Review

The peer review history for this article is available at <https://www.webofscience.com/api/gateway/wos/peer-review/10.1111/bre.70019>.

References

- Alloway, B. V., D. J. Lowe, D. J. Barrell, et al. 2007. "Towards a Climate Event Stratigraphy for New Zealand Over the Past 30 000 Years (NZ-INTIMATE Project)." *Journal of Quaternary Science* 22, no. 1: 9–35.
- Amos, K. J., J. Peakall, P. W. Bradbury, M. Roberts, G. Keevil, and S. Gupta. 2010. "The Influence of Bend Amplitude and Planform Morphology on Flow and Sedimentation in Submarine Channels." *Marine and Petroleum Geology* 27, no. 7: 1431–1447.
- Bailey, W. S., A. D. McArthur, and W. D. McCaffrey. 2021. "Distribution of Contourite Drifts on Convergent Margins: Examples From the Hikurangi Subduction Margin of New Zealand." *Sedimentology* 68, no. 1: 294–323.
- Bailleul, J., F. Chanier, J. Ferrière, et al. 2013. "Neogene Evolution of Lower Trench-Slope Basins and Wedge Development in the Central Hikurangi Subduction Margin, New Zealand." *Tectonophysics* 591: 152–174.
- Bailleul, J., C. Robin, F. Chanier, F. Guillocheau, B. Field, and J. Ferrière. 2007. "Turbidite Systems in the Inner Forearc Domain of the Hikurangi Convergent Margin (New Zealand): New Constraints on the Development of Trench-Slope Basins." *Journal of Sedimentary Research* 77, no. 4: 263–283.
- Bangs, N. L., S. Han, R. Bell, et al. 2022a. *NZ3D Seismic Reflection Data Volume—Prestack Depth Migration (PSDM)*. Marine Geoscience Data System (MGDS). <https://doi.org/10.26022/IEDA/331022>.
- Bangs, N. L., S. Han, R. Bell, et al. 2022b. *NZ3D Velocity Data Volume—3D TTI Full Waveform Inversion (3DTTIFWI)*. Marine Geoscience Data System (MGDS). <https://doi.org/10.26022/IEDA/331023>.
- Bangs, N. L., J. K. Morgan, R. E. Bell, et al. 2023. "Slow Slip Along the Hikurangi Margin Linked to Fluid-Rich Sediments Trailing Subducting Seamounts." *Nature Geoscience* 16, no. 6: 505–512.
- Barker, D. H., R. Sutherland, S. Henrys, and S. Bannister. 2009. "Geometry of the Hikurangi Subduction Thrust and Upper Plate, North Island, New Zealand." *Geochemistry, Geophysics, Geosystems* 10, no. 2: Q02007.
- Barker, D. H. N., S. Henrys, F. Caratori Tontini, et al. 2018. "Geophysical Constraints on the Relationship Between Seamount Subduction, Slow Slip, and Tremor at the North Hikurangi Subduction Zone, New Zealand." *Geophysical Research Letters* 45, no. 23: 12804–12813. <https://doi.org/10.1029/2018gl080259>.
- Barnes, P. M., F. C. Ghisetti, S. Ellis, and J. K. Morgan. 2018. "The Role of Protothrusts in Frontal Accretion and Accommodation of Plate Convergence, Hikurangi Subduction Margin New Zealand." *Geosphere* 14, no. 2: 440–468.
- Barnes, P. M., G. Lamarche, J. Bialas, et al. 2010. "Tectonic and Geological Framework for Gas Hydrates and Cold Seeps on the Hikurangi Subduction Margin New Zealand." *Marine Geology* 272, no. 1–4: 26–48.
- Barnes, P. M., L. M. Wallace, D. M. Saffer, et al. 2020. "Slow Slip Source Characterized by Lithological and Geometric Heterogeneity." *Science Advances* 6, no. 13: eaay3314.
- Barnes, P. M., L. M. Wallace, D. M. Saffer, et al. 2019. *Site U1520. Proceedings of the International Ocean Discovery Program, 372A*. International Ocean Discovery Program.
- Barnes, P., J. Mountjoy, S. Wilcox, S. Mitchell, A. Pallentin, and D. Amyes. 2011. "National Institute of Water and Atmospheric Research (NIWA) Voyage Report, Ocean 2020 Northern Hikurangi Margin Geohazards." NIWA, RV Tangaroa Rep. TAN1114.
- Bell, R., R. Sutherland, D. H. Barker, et al. 2010. "Seismic Reflection Character of the Hikurangi Subduction Interface, New Zealand, in the Region of Repeated Gisborne Slow Slip Events." *Geophysical Journal International* 180, no. 1: 34–48.

- Bourget, J., S. Zaragosi, N. Ellouz-Zimmermann, et al. 2011. "Turbidite System Architecture and Sedimentary Processes Along Topographically Complex Slopes: The Makran Convergent Margin." *Sedimentology* 58, no. 2: 376–406.
- Bourget, J., S. Zaragosi, S. Ellouz-Zimmermann, et al. 2010. "Highstand vs. Lowstand Turbidite System Growth in the Makran Active Margin: Imprints of High-Frequency External Controls on Sediment Delivery Mechanisms to Deep Water Systems." *Marine Geology* 274, no. 1–4: 187–208.
- Brizzi, S., I. van Zelst, F. Funicello, F. Corbi, and Y. van Dinther. 2020. "How Sediment Thickness Influences Subduction Dynamics and Seismicity." *Journal of Geophysical Research: Solid Earth* 125, no. 8: e2019JB018964.
- Buchs, D. M., D. Cukur, H. Masago, and D. Garbe-Schönberg. 2015. "Sediment Flow Routing During Formation of Forearc Basins: Constraints From Integrated Analysis of Detrital Pyroxenes and Stratigraphy in the Kumano Basin, Japan." *Earth and Planetary Science Letters* 414: 164–175.
- Carter, L., and R. M. Carter. 1988. "Late Quaternary Development of Left-Bank-Dominant Levees in the Bounty Trough New Zealand." *Marine Geology* 78, no. 3–4: 185–197.
- Cartigny, M. J., G. Postma, J. H. Van den Berg, and D. R. Mastbergen. 2011. "A Comparative Study of Sediment Waves and Cyclic Steps Based on Geometries, Internal Structures and Numerical Modeling." *Marine Geology* 280, no. 1–4: 40–56.
- Cartigny, M. J., D. Ventra, G. Postma, and J. H. van Den Berg. 2014. "Morphodynamics and Sedimentary Structures of Bedforms Under Supercritical-Flow Conditions: New Insights From Flume Experiments." *Sedimentology* 61, no. 3: 712–748.
- Cattaneo, A., A. Correggiari, T. Marsset, Y. Thomas, B. Marsset, and F. Trincardi. 2004. "Seafloor Undulation Pattern on the Adriatic Shelf and Comparison to Deep-Water Sediment Waves." *Marine Geology* 213, no. 1–4: 121–148.
- Chow, B., Y. Kaneko, and J. Townend. 2022. "Evidence for Deeply Subducted Lower-Plate Seamounts at the Hikurangi Subduction Margin: Implications for Seismic and Aseismic Behavior." *Journal of Geophysical Research: Solid Earth* 127, no. 1: e2021JB022866.
- Clare, M. A., P. J. Talling, and J. E. Hunt. 2015. "Implications of Reduced Turbidity Current and Landslide Activity for the Initial Eocene Thermal Maximum—Evidence From Two Distal, Deep-Water Sites." *Earth and Planetary Science Letters* 420: 102–115.
- Collinson, J. D., and D. B. Thompson. 1982. *Sedimentary Structures*. George Allen & Unwin.
- Collot, J. Y., K. Lewis, G. Lamarche, and S. Lallemand. 2001. "The Giant Ruatōria Debris Avalanche on the Northern Hikurangi Margin, New Zealand: Result of Oblique Seamount Subduction." *Journal of Geophysical Research: Solid Earth* 106, no. B9: 19271–19297.
- Couvin, B., A. Georgiopoulou, J. J. Mountjoy, et al. 2020. "A New Depositional Model for the Tuaheni Landslide Complex, Hikurangi Margin, New Zealand." *Geological Society, London, Special Publications* 500, no. 1: 551–566. <https://doi.org/10.1144/sp500-2019-180>.
- Covault, J. A., and S. A. Graham. 2010. "Submarine Fans at All Sea-Level Stands: Tectono-Morphologic and Climatic Controls on Terrigenous Sediment Delivery to the Deep Sea." *Geology* 38, no. 10: 939–942.
- Covault, J. A., E. Shelef, M. Traer, S. M. Hubbard, B. W. Romans, and A. Fildani. 2012. "Deep-Water Channel Run-Out Length: Insights From Seafloor Geomorphology." *Journal of Sedimentary Research* 82, no. 1: 21–36.
- Crundwell, M. P., and A. Woodhouse. 2022. "Biostratigraphically Constrained Chronologies for Quaternary Sequences From the Hikurangi Margin of North-Eastern Zealandia." *New Zealand Journal of Geology and Geophysics* 67, no. 3: 364–384.
- Davidson, S. R., P. M. Barnes, J. R. Pettinga, A. Nicol, J. J. Mountjoy, and S. A. Henrys. 2020. "Conjugate Strike-Slip Faulting Across a Subduction Front Driven by Incipient Seamount Subduction." *Geology* 48, no. 5: 493–498.
- Ellis, S., Å. Fagereng, D. Barker, et al. 2015. "Fluid Budgets Along the Northern Hikurangi Subduction Margin, New Zealand: The Effect of a Subducting Seamount on Fluid Pressure." *Geophysical Journal International* 202, no. 1: 277–297.
- Gase, A. C., N. L. Bangs, D. M. Saffer, et al. 2023. "Subducting Volcaniclastic-Rich Upper Crust Supplies Fluids for Shallow Megathrust and Slow Slip." *Science Advances* 9, no. 33: eadh0150.
- Ghissetti, F. C., P. M. Barnes, S. Ellis, A. A. Plaza-Faverola, and D. H. Barker. 2016. "The Last 2 Myr of Accretionary Wedge Construction in the Central Hikurangi Margin (North Island, New Zealand): Insights From Structural Modeling." *Geochemistry, Geophysics, Geosystems* 17, no. 7: 2661–2686.
- Heuret, A., C. P. Conrad, F. Funicello, S. Lallemand, and L. Sandri. 2012. "Relation Between Subduction Megathrust Earthquakes, Trench Sediment Thickness and Upper Plate Strain." *Geophysical Research Letters* 39, no. 5: L05304.
- Hiscott, R. N., F. R. Hall, and C. Pirmez. 1997. "Turbidity-Current Overspill From the Amazon Channel: Texture of the Silt/Sand Load, Paleoflow From Anisotropy of Magnetic Susceptibility, and Implications for Flow Processes." In *Proceedings-Ocean Drilling Program Scientific Results*, edited by R. D. Flood, D. J. W. Pipe, A. Klaus, and L. C. Peterson, vol. 155, 53–78. Ocean Drilling Program.
- Hodgson, D. M., J. Peakall, and K. L. Maier. 2022. "Submarine Channel Mouth Settings: Processes, Geomorphology, and Deposits." *Frontiers in Earth Science* 10: 790320.
- Howarth, J. D., A. R. Orpin, Y. Kaneko, et al. 2021. "Calibrating the Marine Turbidite Palaeoseismometer Using the 2016 Kaikōura Earthquake." *Nature Geoscience* 14, no. 3: 161–167.
- Kane, I. A., M. A. Clare, E. Miramontes, et al. 2020. "Seafloor Microplastic Hotspots Controlled by Deep-Sea Circulation." *Science* 368, no. 6495: 1140–1145.
- Kelly, R. W., R. M. Dorrell, A. D. Burns, and W. D. McCaffrey. 2019. "The Structure and Entrainment Characteristics of Partially Confined Gravity Currents." *Journal of Geophysical Research: Oceans* 124, no. 3: 2110–2125.
- Kneller, B., M. M. Nasr-Azadani, S. Radhakrishnan, and E. Meiburg. 2016. "Long-Range Sediment Transport in the World's Oceans by Stably Stratified Turbidity Currents." *Journal of Geophysical Research: Oceans* 121, no. 12: 8608–8620.
- Kostic, S., and G. Parker. 2006. "The Response of Turbidity Currents to a Canyon–Fan Transition: Internal Hydraulic Jumps and Depositional Signatures." *Journal of Hydraulic Research* 44, no. 5: 631–653.
- Kroeger, K. F., G. J. Crutchley, R. Kellett, and P. M. Barnes. 2019. "A 3-D Model of Gas Generation, Migration, and Gas Hydrate Formation at a Young Convergent Margin (Hikurangi Margin, New Zealand)." *Geochemistry, Geophysics, Geosystems* 20, no. 11: 5126–5147.
- Lewis, K. B. 1993. "The Emerging, Imbricate Frontal Wedge of the Hikurangi Margin." *Sedimentary Basins of the World* 2: 225.
- Lewis, K. B. 1994. "The 1500-Km-Long Hikurangi Channel: Trench-Axis Channel That Escapes Its Trench, Crosses a Plateau, and Feeds a Fan Drift." *Geo-Marine Letters* 14: 19–28.
- Lewis, K. B., and P. M. Barnes. 1999. "Kaikōura Canyon, New Zealand: Active Conduit From Near-Shore Sediment Zones to Trench-Axis Channel." *Marine Geology* 162, no. 1: 39–69.
- Lewis, K. B., J. Y. Collot, and S. E. Lallemand. 1998. "The Dammed Hikurangi Trough: A Channel-Fed Trench Blocked by Subducting Seamounts and Their Wake Avalanches (New Zealand–France GeodyNZ Project)." *Basin Research* 10, no. 4: 441–468.

- Lewis, K. B., and H. M. Pantin. 2002. "Channel-Axis, Overbank and Drift Sediment Waves in the Southern Hikurangi Trough New Zealand." *Marine Geology* 192, no. 1–3: 123–151.
- Lewis, K. B. 2001. "Voyage Report TAN0106." National Institute of Water and Atmospheric Research.
- Maier, K. L., S. Nodder, P. Gerring, et al. 2022. *TAN2207 Voyage Report, Marsden Organic Carbon 1, Deployment 15–25 June 2022*. National Institute of Water and Atmospheric Research, Report MFR21302.
- Maier, K. L., L. J. Strachan, S. Tickle, A. R. Orpin, S. D. Nodder, and J. Howarth. 2024. "Testing Turbidite Conceptual Models With the Kaikōura Earthquake Co-Seismic Event Bed, Aotearoa New Zealand." *Journal of Sedimentary Research* 94: 325–333.
- McArthur, A. D., A. Crisóstomo-Figueroa, A. Wunderlich, A. Karvelas, and W. D. McCaffrey. 2022. "Sedimentation on Structurally Complex Slopes: Neogene to Recent Deep-Water Sedimentation Patterns Across the Central Hikurangi Subduction Margin, New Zealand." *Basin Research* 34, no. 5: 1807–1837.
- McArthur, A. D., and D. E. Tek. 2021. "Controls on the Origin and Evolution of Deep-Ocean Trench-Axial Channels." *Geology* 49, no. 8: 883–888.
- McArthur, A. D., D. E. Tek, M. Poyatos-Moré, L. Colombera, and W. D. McCaffrey. 2024. "Deep-Ocean Channel-Wall Collapse Order of Magnitude Larger Than any Other Documented." *Communications Earth & Environment* 5, no. 1: 143.
- McDonald, L. S., L. J. Strachan, K. Holt, et al. 2024. "Using Pollen in Turbidites for Vegetation Reconstructions." *Journal of Quaternary Science* 39, no. 7: 1053–1063. <https://doi.org/10.1002/jqs.3653>.
- Mitchum, R. M., Jr. 1977. "Seismic Stratigraphy and Global Changes of Sea Level: Part 11. Glossary of Terms Used in Seismic Stratigraphy: Section 2. Application of Seismic Reflection Configuration to Stratigraphic Interpretation." In *AAPG Memoir*, edited by O. R. Berg and D. G. Woolverton, vol. 26. 205–212. AAPG.
- Mochizuki, K., R. Sutherland, S. Henrys, et al. 2019. "Recycling of Depleted Continental Mantle by Subduction and Plumes at the Hikurangi Plateau Large Igneous Province, Southwestern Pacific Ocean." *Geology* 47, no. 8: 795–798.
- Mountjoy, J. J., J. D. Howarth, A. R. Orpin, et al. 2018. "Earthquakes Drive Large-Scale Submarine Canyon Development and Sediment Supply to Deep-Ocean Basins." *Science Advances* 4, no. 3: eaar3748.
- Mutti, E. 1977. "Distinctive Thin-Bedded Turbidite Facies and Related Depositional Environments in the Eocene Hecho Group (South-Central Pyrenees, Spain)." *Sedimentology* 24, no. 1: 107–131.
- Noda, A., A. Greve, A. Woodhouse, and M. Crundwell. 2024. "Depositional Rate, Grain Size and Magnetic Mineral Sulfidization in Turbidite Sequences, Hikurangi Margin, New Zealand." *New Zealand Journal of Geology and Geophysics* 67, no. 3: 288–311.
- Omura, A., K. Ikehara, K. Arai, and Udrehk. 2017. "Determining Sources of Deep-Sea Mud by Organic Matter Signatures in the Sunda Trench and Aceh Basin Off Sumatra." *Geo-Marine Letters* 37: 549–559.
- Orpin, A. R. 2004. "Holocene Sediment Deposition on the Poverty-Slope Margin by the Muddy Waipaoa River, East Coast New Zealand." *Marine Geology* 209, no. 1–4: 69–90.
- Paull, C. K., M. McGann, E. J. Sumner, et al. 2014. "Sub-Decadal Turbidite Frequency During the Early Holocene: Eel Fan, Offshore Northern California." *Geology* 42, no. 10: 855–858.
- Peakall, J., I. A. Kane, D. G. Masson, G. Keevil, W. McCaffrey, and R. Corney. 2012. "Global (Latitudinal) Variation in Submarine Channel Sinuosity." *Geology* 40, no. 1: 11–14.
- Pecher, I. A., P. M. Barnes, L. J. Levay, and E. Scientists. 2018. *Expedition 372 Preliminary Report: Creeping Gas Hydrate Slides and Hikurangi LWD*. Vol. 372. International Ocean Discovery Program.
- Pedley, K. L., P. M. Barnes, J. R. Pettinga, and K. B. Lewis. 2010. "Seafloor Structural Geomorphic Evolution of the Accretionary Frontal Wedge in Response to Seamount Subduction, Poverty Indentation New Zealand." *Marine Geology* 270, no. 1–4: 119–138.
- Pilkey, O. H., D. M. Bush, and R. W. Rodriguez. 1988. "Carbonate-Terrigenous Sedimentation on the North Puerto Rico Shelf." In *Developments in Sedimentology*, edited by L. J. Doyle and H. H. Roberts, vol. 42, 231–250. Elsevier.
- Piper, D. J., R. von Huene, and J. R. Duncan. 1973. "Late Quaternary Sedimentation in the Active Eastern Aleutian Trench." *Geology* 1, no. 1: 19–22.
- Pizer, C. O., J. D. Howarth, K. J. Clark, et al. 2024. "Integrated Onshore–Offshore Paleoseismic Records Show Multiple Slip Styles on the Plate Interface, Central Hikurangi Subduction Margin, Aotearoa New Zealand." *Quaternary Science Reviews* 344: 108942.
- Plaza-Faverola, A., D. Klaeschen, P. Barnes, I. Pecher, S. Henrys, and J. Mountjoy. 2012. "Evolution of Fluid Expulsion and Concentrated Hydrate Zones Across the Southern Hikurangi Subduction Margin, New Zealand: An Analysis From Depth Migrated Seismic Data." *Geochemistry, Geophysics, Geosystems* 13, no. 8: Q08018.
- Pohl, F., J. T. Eggenhuisen, M. Tilston, and M. J. B. Cartigny. 2019. "New Flow Relaxation Mechanism Explains Scour Fields at the End of Submarine Channels." *Nature Communications* 10, no. 1: 4425.
- Pope, E. L., M. S. Heijnen, P. J. Talling, et al. 2022. "Carbon and Sediment Fluxes Inhibited in the Submarine Congo Canyon by Landslide-Damming." *Nature Geoscience* 15, no. 10: 845–853.
- Postma, G., and M. J. Cartigny. 2014. "Supercritical and Subcritical Turbidity Currents and Their Deposits—A Synthesis." *Geology* 42, no. 11: 987–990.
- Pouderoux, H., J. N. Proust, and G. Lamarche. 2014. "Submarine Paleoseismology of the Northern Hikurangi Subduction Margin of New Zealand as Deduced From Turbidite Record Since 16 Ka." *Quaternary Science Reviews* 84: 116–131.
- Pouderoux, H., J. N. Proust, G. Lamarche, A. Orpin, and H. Neil. 2012. "Postglacial (After 18 Ka) Deep-Sea Sedimentation Along the Hikurangi Subduction Margin (New Zealand): Characterisation, Timing and Origin of Turbidites." *Marine Geology* 295: 51–76.
- Reading, H. G. 1996. *Sedimentary Environments: Processes, Facies and Stratigraphy*. 3rd ed. Blackwell Publishing.
- Saffer, D. M., and L. M. Wallace. 2015. "The Frictional, Hydrologic, Metamorphic and Thermal Habitat of Shallow Slow Earthquakes." *Nature Geoscience* 8, no. 8: 594–600.
- Saffer, D. M., L. M. Wallace, P. M. Barnes, et al. 2019. "Expedition 372B/375 Summary." In *Proceedings of the International Ocean Discovery Program*, edited by L. M. Wallace, D. M. Saffer, P. M. Barnes, et al. vol. 372, 1–35. International Ocean Discovery Program.
- Sangree, J. B., and J. M. Widmier. 1979. "Interpretation of Depositional Facies From Seismic Data." *Geophysics* 44, no. 2: 131–160.
- Sequeiros, O. E. 2012. "Estimating Turbidity Current Conditions From Channel Morphology: A Froude Number Approach." *Journal of Geophysical Research: Oceans* 117, no. C4: C04003.
- Shanmugam, G. 1988. "Origin, Recognition, and Importance of Erosional Unconformities in Sedimentary Basins." In *New Perspectives in Basin Analysis*, edited by K. L. Kleinspehn and C. Paola, 83–108. Springer.
- Shumaker, L. E., Z. R. Jobe, S. A. Johnstone, L. A. Pettinga, D. Cai, and J. D. Moody. 2018. "Controls on Submarine Channel-Modifying Processes Identified Through Morphometric Scaling Relationships." *Geosphere* 14, no. 5: 2171–2187.

- Skarbek, R. M., A. W. Rempel, and D. A. Schmidt. 2012. "Geologic Heterogeneity Can Produce Aseismic Slip Transients." *Geophysical Research Letters* 39, no. 21: L21306.
- Slootman, A., and M. J. Cartigny. 2020. "Cyclic Steps: Review and Aggradation-Based Classification." *Earth-Science Reviews* 201: 102949.
- Sømme, T. O., O. J. Martinsen, and J. B. Thurmond. 2009. "Reconstructing Morphological and Depositional Characteristics in Subsurface Sedimentary Systems: An Example From the Maastrichtian-Danian Ormen Lange System, More Basin, Norwegian Sea." *American Association of Petroleum Geologists Bulletin* 93, no. 10: 1347–1377.
- Spinewine, B., O. E. Sequeiros, M. H. Garcia, et al. 2009. "Experiments on Wedge-Shaped Deep Sea Sedimentary Deposits in Minibasins and/or on Channel Levees Emplaced by Turbidity Currents. Part II. Morphodynamic Evolution of the Wedge and of the Associated Bedforms." *Journal of Sedimentary Research* 79, no. 8: 608–628.
- Stevenson, C. J., C. A. L. Jackson, D. M. Hodgson, S. M. Hubbard, and J. T. Eggenhuisen. 2015. "Deep-Water Sediment Bypass." *Journal of Sedimentary Research* 85, no. 9: 1058–1081.
- Stow, D. A. 1985. "Fine-Grained Sediments in Deep Water: An Overview of Processes and Facies Models." *Geo-Marine Letters* 5: 17–23.
- Sweet, M. L., and M. D. Blum. 2016. "Connections Between Fluvial to Shallow Marine Environments and Submarine Canyons: Implications for Sediment Transfer to Deep Water." *Journal of Sedimentary Research* 86, no. 10: 1147–1162.
- Symons, W. O., E. J. Sumner, P. J. Talling, M. J. Cartigny, and M. A. Clare. 2016. "Large-Scale Sediment Waves and Scours on the Modern Seafloor and Their Implications for the Prevalence of Supercritical Flows." *Marine Geology* 371: 130–148.
- Talling, P. J., J. Allin, D. A. Armitage, et al. 2015. "Key Future Directions for Research on Turbidity Currents and Their Deposits." *Journal of Sedimentary Research* 85, no. 2: 153–169.
- Talling, P. J., L. A. Amy, and R. B. Wynn. 2007. "New Insight Into the Evolution of Large-Volume Turbidity Currents: Comparison of Turbidite Shape and Previous Modelling Results." *Sedimentology* 54, no. 4: 737–769.
- Talling, P. J., M. J. Cartigny, E. Pope, et al. 2023. "Detailed Monitoring Reveals the Nature of Submarine Turbidity Currents." *Nature Reviews Earth and Environment* 4, no. 9: 642–658.
- Talling, P. J., D. G. Masson, E. J. Sumner, and G. Malgesini. 2012. "Subaqueous Sediment Density Flows: Depositional Processes and Deposit Types." *Sedimentology* 59, no. 7: 1937–2003.
- Tek, D. E., A. D. McArthur, M. Poyatos-Moré, et al. 2022. "Controls on the Architectural Evolution of Deep-Water Channel Overbank Sediment Wave Fields: Insights From the Hikurangi Channel, Offshore New Zealand." *New Zealand Journal of Geology and Geophysics* 65, no. 1: 141–178.
- Tek, D. E., A. D. McArthur, M. Poyatos-Moré, et al. 2021. "Relating Seafloor Geomorphology to Subsurface Architecture: How Mass-Transport Deposits and Knickpoint-Zones Build the Stratigraphy of the Deep-Water Hikurangi Channel." *Sedimentology* 68, no. 7: 3141–3190.
- Traer, M. M., A. Fildani, O. Fringer, T. McHargue, and G. E. Hilley. 2018. "Turbidity Current Dynamics: I. Model Formulation and Identification of Flow Equilibrium Conditions Resulting From Flow Stripping and Overspill." *Journal of Geophysical Research: Earth Surface* 123, no. 3: 501–519.
- Underwood, M. B. 1986. "Transverse Infilling of the Central Aleutian Trench by Unconfined Turbidity Currents." *Geo-Marine Letters* 6: 7–13.
- Underwood, M. B. 2007. "Sediment Inputs to Subduction Zones: Why Lithostratigraphy and Clay Mineralogy Matter." In *The Seismogenic Zone of Subduction Thrust Faults*, edited by T. H. Dixon and J. C. Moore, 42–85. Columbia University Press.
- Underwood, M. B. 2023. "Composition of Fine-Grained Sediment in the Hikurangi Trough: Evidence for Intermingling Among Axial Gravity Flows, Transverse Gravity Flows and Margin-Parallel Ocean Currents." *Sedimentology* 70, no. 3: 828–864.
- Underwood, M. B., and D. E. Karig. 1980. "Role of Submarine Canyons in Trench and Trench-Slope Sedimentation." *Geology* 8, no. 9: 432–436.
- Upton, P., A. J. Kettner, B. Gomez, A. R. Orpin, N. Litchfield, and M. J. Page. 2013. "Simulating Post-LGM Riverine Fluxes to the Coastal Zone: The Waipaoa River System, New Zealand." *Computers & Geosciences* 53: 48–57.
- Veeken, P., and B. Van Moerkerken. 2013. "Seismic Stratigraphic Techniques." In *Seismic Stratigraphy and Depositional Facies Models*, edited by P. C. Veeken, 105–214. Elsevier.
- Völker, D., J. Geersen, E. Contreras-Reyes, and C. Reichert. 2013. "Sedimentary Fill of the Chile Trench (32–46S): Volumetric Distribution and Causal Factors." *Journal of the Geological Society* 170, no. 5: 723–736.
- Wallace, L. M., J. Beavan, R. McCaffrey, and D. Darby. 2004. "Subduction Zone Coupling and Tectonic Block Rotations in the North Island, New Zealand." *Journal of Geophysical Research: Solid Earth* 109, no. B12: B12406.
- Wallace, L. M., D. M. Saffer, P. M. Barnes, I. A. Pecher, K. E. Petronotis, and L. J. LeVay. 2019. "Hikurangi Subduction Margin Coring, Logging, and Observatories." Proceedings of the International Ocean Discovery Program, 372.
- Wang, W., M. K. Savage, A. Yates, et al. 2022. "Temporal Velocity Variations in the Northern Hikurangi Margin and the Relation to Slow Slip." *Earth and Planetary Science Letters* 584: 117443.
- Watson, S. J., J. J. Mountjoy, and G. J. Crutchley. 2020. "Tectonic and Geomorphic Controls on the Distribution of Submarine Landslides Across Active and Passive Margins, Eastern New Zealand." *Geological Society, London, Special Publications* 500, no. 1: 477–494.
- Wells, M. G., and R. M. Dorrell. 2021. "Turbulence Processes Within Turbidity Currents." *Annual Review of Fluid Mechanics* 53, no. 1: 59–83.
- Woodhouse, A., P. M. Barnes, A. Shorrock, et al. 2022. "Trench Floor Depositional Response to Glacio-Eustatic Changes Over the Last 45 Ka, Northern Hikurangi Subduction Margin, New Zealand." *New Zealand Journal of Geology and Geophysics* 67, no. 3: 312–335.
- Wynn, R. B., and D. A. Stow. 2002. "Classification and Characterisation of Deep-Water Sediment Waves." *Marine Geology* 192, no. 1–3: 7–22.
- Zuffa, G. G., W. R. Normark, F. Serra, and C. A. Brunner. 2000. "Turbidite Megabeds in an Oceanic Rift Valley Recording Jökulhlaups of Late Pleistocene Glacial Lakes of the Western United States." *Journal of Geology* 108, no. 3: 253–274.

Supporting Information

Additional supporting information can be found online in the Supporting Information section.